SCIEPublish

Review

A Review on the Application of Nanomaterials to Boost the Service Performances of Carbon-Containing Refractories

Junyi Lv, Haijun Zhang, Haohui Gu and Feng Liang *

The State Key Laboratory of Refractories and Metallurgy, Wuhan University of Science and Technology, Wuhan 430081, China; lvjunyi@wust.edu.cn (J.L.); zhanghaijun@wust.edu.cn (H.Z.); 1342584102@qq.com (H.G.)

* Corresponding author. E-mail: liangfengref@wust.edu.cn (F.L.)

Received: 4 August 2024; Accepted: 27 August 2024; Available online: 2 September 2024

ABSTRACT: To meet the high-quality requirements for clean steel production and fully exploit the performance advantages of carbon-containing refractories, nanomaterial has been introduced into the matrix to develop advanced carbon-containing refractories. Nanomaterials, as critical additives, play a crucial role in developing novel refractories. The service performances of carbon-containing refractories are affected not only by their physical and chemical properties but also by their microstructure. This review provides a comprehensive overview of the latest research on oxide-carbon composite refractories containing nanomaterials, categorized by their composition: nanocarbons, nano oxides, and nano non-oxides. Incorporating nanomaterials can enhance the service performances of the refractories, optimizing phase composition and microstructure. Furthermore, future research directions in nanomaterial technology for carbon-containing refractories are discussed.

Keywords: Carbon-containing refractory; Nanomaterial; Microstructure; Service performance

1. Introduction

Carbon-containing refractories (CCRs) play a crucial role in the iron and steel metallurgy process due to their outstanding thermal shock and slag resistance [1–7]. These refractories are manufactured using aggregates primarily composed of one or more high melting-point oxides or their associated mineral phases. Carbon, noted for its exceptional refractory properties such as non-wettability by slag and high thermal conductivity, can be incorporated into CCRs either as an additive or as a binder (e.g., coal tar, petroleum pitch, or resin) [8–10]. The integration of carbon into oxide aggregates results in various types of CCRs, including magnesia−carbon (MgO−C) [11,12], calcia−magnesia−carbon (CaO−MgO−C) [13], alumina−carbon (Al_2O_3−C) [14], zirconia−carbon (ZrO_2−C) [15,16], and alumina silicon carbide−carbon (Al_2O_3−SiC−C) [17,18].

Carbon-containing calcia, magnesia and doloma (sintered dolomite) are classified as basic oxide refractories. MgO−C refractories are widely used as lining materials for converters, electric arc furnaces, and the slag lines of steel ladles. Doloma-carbon refractory bricks find extensive application in the steel industry for lining basic oxygen furnace converters, ladle furnaces, and electric arc furnaces [19,20]. A significant drawback of basic refractories is their tendency to hydrate. However, including carbon enhances thermal shock resistance, reduces porosity, increases the wetting angle, and significantly improves hydration resistance [21–23]. Non-basic oxide-carbon refractories, such as carbon-containing alumina, alumina−silicon carbide, and zirconia, are frequently used in iron and steelmaking. Al_2O_3−C refractories are primarily employed in producing continuous casting components, including slide plates, submerged entry nozzles, long nozzles, and monobloc stoppers [24,25]. ZrO_2−C refractories, known for their superior resistance to abrasion and corrosion, are used in hollow ware like continuous casting submerged entry nozzles [26–28]. Al_2O_3−SiC−C refractories are mainly used in torpedoes to transfer liquid iron and steel ladles [29–31]. Graphite is the primary carbon source in CCRs because it enhances slag corrosion resistance. This enhancement occurs through the reaction of graphite with oxides in slag and impurities within the brick, forming gaseous products. These gaseous

https://doi.org/10.70322/htm.2024.10005

products are then re-oxidized, resulting in a dense deposit of the secondary oxide phase at the slag-refractory interface, which prevents melt penetration [32–34].

Oxide-carbon refractories represent a significant advancement in stainless steel manufacturing, contributing to a marked reduction in refractory consumption [35,36]. However, traditional oxide-carbon refractories with a high carbon content present several drawbacks:

(1) Molten metal, such as steel, can absorb carbon from the CCRs, resulting in an undesirable increase in the carbon content of the metal, which is detrimental to producing high-quality steel.
(2) The high graphite content, coupled with high thermal conductivity, can lower the temperature of the molten metal, adversely affecting the tapping process.
(3) Graphite's tendency to be oxidized creates pores in the refractory bodies, accelerating slag corrosion and releasing CO_x greenhouse gases.

Hence, reducing the carbon content in oxide-carbon refractories is essential to mitigate the negative impacts on high-quality steel production. However, lowering carbon content adversely affects the refractories' properties. When carbon content drops below 5 wt.%, thermal diffusivity decreases and thermal expansion increases, significantly impairing the refractories' thermal shock and slag corrosion resistance.

In recent years, to address the problems and challenges of CCRs, researchers have investigated the effects of various types of nanomaterials on the service performances of the refractories [37–40]. Nanoscale additives were proposed in refractories as early as 2003 [41,42]. Further investigations have demonstrated that adding small amounts of nanoscale materials can significantly enhance the performance of refractories [43–45]. Nanomaterials used as ingredients in CCRs are divided into two categories: active and inert materials. Inert nanomaterials primarily enhance CCR properties through nucleation, filler, and bridging effects. In contrast, active nanomaterials influence the in situ generation of new phases and nucleation as well as filler effects. Additionally, the optimal amounts of nanomaterials needed for achieving the best refractory performance vary with the geometric sizes, shapes, and physical properties.

This review thoroughly examined recent developments in oxide-carbon refractories reinforced with nanomaterial additives. The categories of nanomaterial additives, including nanocarbons, nano oxides, and nano non-oxide and the performances of reinforced oxide-carbon composites, are extensively discussed (Figure 1). Based on this review, some future research trends in the field of oxide-carbon refractories are proposed.

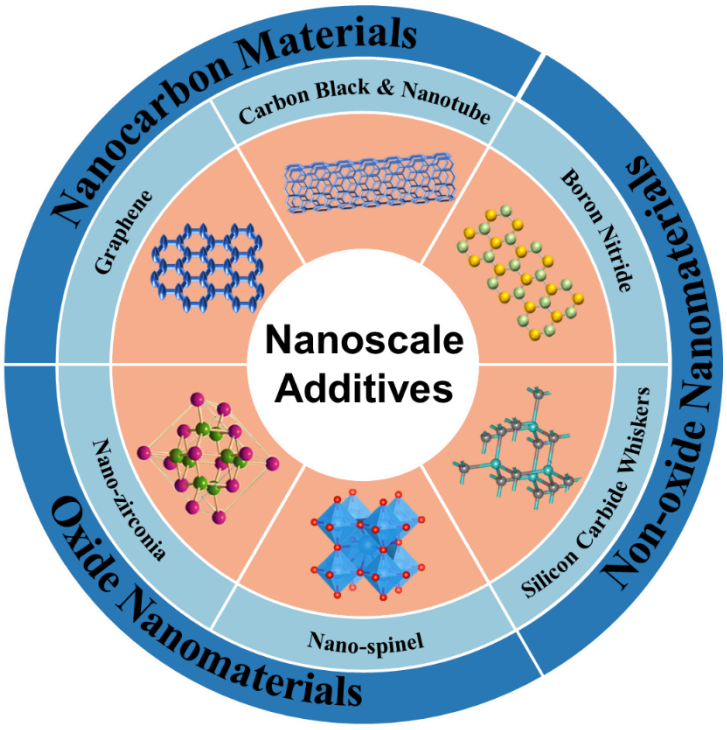

Figure 1. Category of nanomaterial additives.

2. Nanocarbon Containing Refractories

Nanocarbon sources used in oxide-carbon refractories include carbon black (CB), graphite nanosheets (GNSs), and carbon nanotubes (CNTs). These nanocarbons can easily fill the voids between coarse, medium, and fine particles, thereby promoting the formation of ceramic bonding phases. This process reduces porosity and enhances density, strength and corrosion resistance in the final refractory products [46–49].

2.1. Carbon Black Containing Refractories

Carbon black consisting of nanosized particles (approximately 30 nm) in the form of porous and compressible agglomerate, is widely used in structural composites. The addition of CB into refractories results in improved properties [50–54], and the advantages associated with the addition of CB are as follows: (1) filling the gaps between other refractory components, thereby enhancing density; (2) contributing to the in situ formation of carbide phases due to its high reactivity; and (3) increasing the carbon content, which is essential for boosting the performances of CCRs.

Different nanosized carbon sources result in various properties due to their size and particle size distribution. Pilli et al. [55] prepared low carbon-containing Al_2O_3−C refractories using two different grades of CB, namely, N220 (particle size 20–25 nm) and N990 (particle size ~250 nm). As shown in the fracture surface of the sample in Figure 2a, the nanocarbon−containing sample coked at 1000 °C exhibited a columnar or needle-like structure, attributed to forming aluminum carbide ceramic phases. The formation of in situ ceramic phases in nanocarbon-containing compositions provided a compact microstructure that improved strength, inhibited oxidation, and contributed to corrosion resistance. Figure 2b shows the cold crushing strength (CCS) of samples with different particle sizes of nanocarbon black. It could be seen that the batch containing 0.5 wt.% N220 exhibited higher strength values, which might be due to the higher reactivity of nanocarbon forming more carbides. However, excessive content of nanocarbon black could cause agglomeration and the particles might not fill the gaps between alumina particles, negatively impacting density and strength. Additionally, after three thermal shock cycles, the strength retention ratio of samples containing nanocarbon (3 wt.% flake graphite + 1.0 wt.% nanocarbon black) was higher than that of samples with 25 wt.% flake graphite (Figure 2c). Similarly, Wu et al. [56] found minimal corrosion and penetration under a reducing atmosphere for Al_2O_3−SiC−C castables with 0.4 wt.% CB. However, the porosity increased with the CB content. Li et al. [57] developed Al_2O_3−C refractories with excellent mechanical properties and thermal shock resistance by combining nano CB and MWCNTs. The improvement was attributed to the filling effect and thermal stress absorption of the nano CB, while MWCNTs reinforced and toughened the matrix of the refractories. Liao et al. [58] dispersed carbon black (CB) particles into reactive alumina powders using planetary ball milling with ethanol as the dispersion medium. The pre-mixed fine powders were then used to fabricate Al_2O_3−C refractories, resulting in refractories with a higher cold modulus of rupture (CMOR) and superior thermal shock resistance. Bag et al. [59] investigated the impact of nano CB content on the properties of MgO−C refractories while maintaining the total carbon content at less than half that of traditional MgO−C refractories. They determined that the optimal properties were achieved by adding 0.9 wt.% nano CB in combination with 3 wt.% graphite. The incorporation of nano CB resulted in a more uniformly dispersed matrix and enhanced filling of the microscopic spaces between coarse, medium, and fine particles in the starting materials. Additionally, the nano CB improved the slag corrosion resistance by increasing wettability resistance.

The application of nanoscale materials in carbon-bonded refractories has faced significant obstacles due to their extremely high production costs and the difficulty of achieving homogeneous distribution within the refractory matrix [60]. Research suggests that preparing oxide or carbide coatings with enhanced water wettability on nanocarbon raw materials can aid their uniform dispersion in refractories. Ye et al. [61] employed a molten salt synthesis (MSS) technique to prepare SiC coatings on CB particles. The SiC-coated CB particles exhibited significantly enhanced dispersity and flowability in water compared to their uncoated counterparts. The apparent viscosity of a water suspension containing SiC-coated CB was notably lower than that of the suspension with uncoated CB. Najafi [62] introduced CB (N110) into MgO−C refractory bricks using $Mg(OH)_2$/CB mixture as a starting material. The SEM image in Figure 2d clearly showed that CB nanoparticles are located between MgO particles, indicating that the sol−gel method allowed CB nanoparticles to be well dispersed and stabilized in $Mg(OH)_2$, preventing their severe agglomeration. The SEM image in Figure 2e showed no significant microstructural defects in the MgO−C refractory matrix can be observed, and the main refractory components (MgO and graphite) were well bonded with each other. The CCS results showed that adding 1 wt.% of the nano-admixture increased the CCS value by over 100%, demonstrating its excellent mechanical properties (Figure 2f). This indicates that highly dispersed CB nanoparticles significantly enhance the mechanical and physical properties of industrial MgO−C refractory bricks.

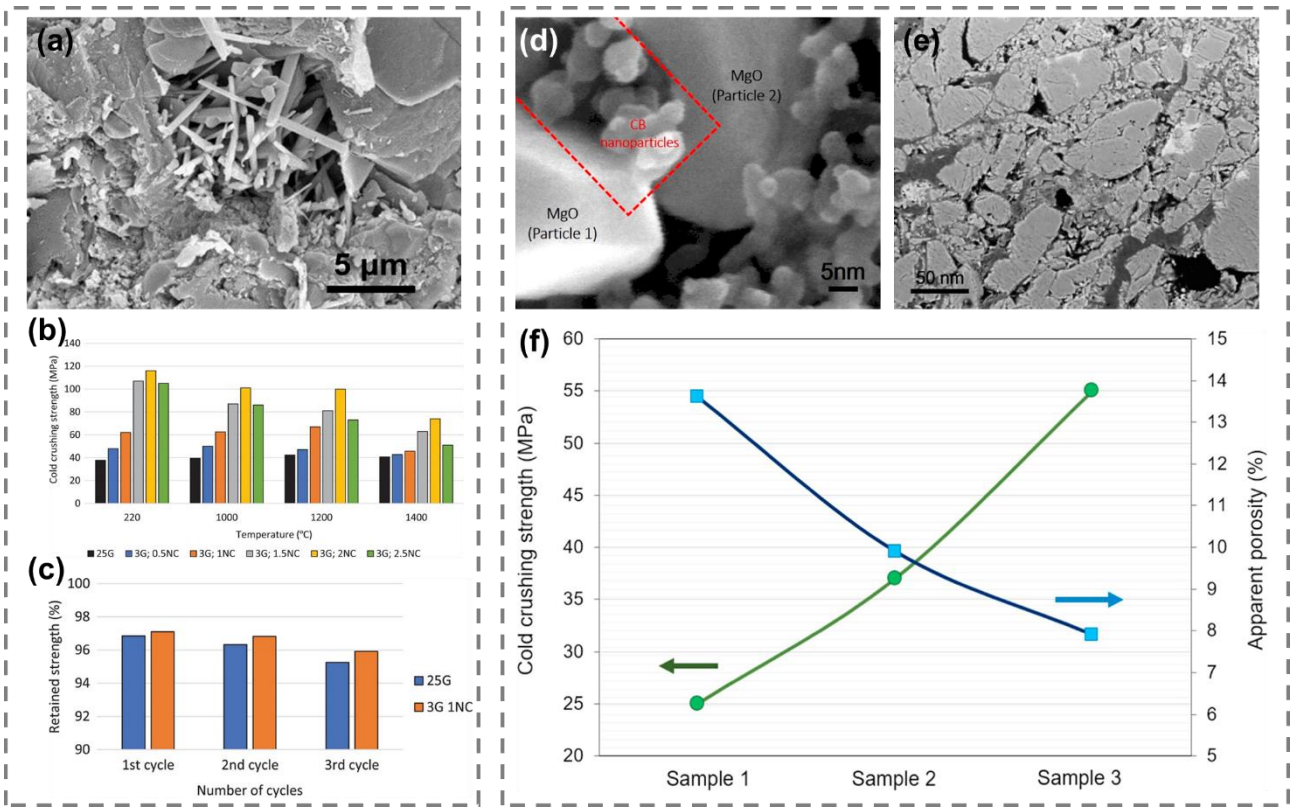

Figure 2. (**a**) SEM image of the refractory sample containing 3 wt.% flake graphite and 2 wt.% nanocarbon black after coked at 1000 °C. (**b**) Cold compressive strength of the sample was achieved with the addition of N220 nanocarbon black. (**c**) Retained strength of the sample with 25 wt.% flake graphite and the sample with 3 wt.% flake graphite and 1 wt.% nanocarbon black [55]. (**d**) SEM micrograph of the nano-MgO/carbon black mixture. (**e**) SEM micrograph of the MgO−C refractory sample with 1 wt.% MgO/carbon black nanocomposite addition. And (**f**) cold crushing strength and apparent porosity results of MgO−C refractory bricks with different amounts of nano-admixture [62]. (**a**–**c**) Copyright 2022, John Wiley and Sons; (**d**–**f**) Copyright 2016, Elsevier.

As an amorphous phase, the CB's oxidation resistance and thermal conductivity are not as good as those of graphite flakes, which limits its application in CCRs. Therefore, enhancing the oxidation resistance of CB will help to expand the application prospects and address an urgent need for CCRs. To improve oxidation resistance, the effects of adding various antioxidants were studied [63–69]. Behera et al. [70] discovered that incorporating metal powders as antioxidants increases the formation of in situ ceramic phases, attributed to the higher surface area and reactivity of N220 nanocarbon compared to graphite. Among the antioxidants studied, aluminum was the most effective. This effectiveness is due to the uniform formation of in situ ceramic phases, such as aluminum carbide and magnesium aluminate spinel.

2.2. Carbon Nanotubes Containing Refractories

CNTs are seamless cylinders formed by wrapping graphene sheets, with carbon atoms covalently bonded through sp^2 hybridization. These structures have been extensively studied due to their remarkable physical and chemical properties [71–73]. CNTs exhibit exceptional strength along the axial direction, with Young's modulus ranging from 270 to 950 GPa and tensile strength between 11 and 63 GPa. Additionally, their smaller particle size and high specific surface area enable CNTs to effectively fill pores or gaps in the refractory matrix, promoting the formation of ceramic bonding phases and enhancing mechanical properties [74–77].

Due to their outstanding physical, chemical, and mechanical properties, CNTs are a promising carbon source to partially or completely replace graphite flakes in CCRs. Halder et al. [78] partially substituted graphite with amorphous CNTs to reduce the total carbon content while maintaining the same or greater carbon surface area. The incorporation of CNTs improved the compactness of the refractory composite and decreased the cumulative volume of large pores. Additionally, the partial substitution of graphite with CNTs generated a more effective surface area due to the lower density of CNTs, significantly enhancing slag corrosion resistance in specimens containing 0.18 wt.% CNTs. Luo et al. [79] investigated the effects of multi-walled CNTs (MWCNTs) on the microstructures and mechanical properties of Al_2O_3−C refractories. The addition of 0.05 wt.% MWCNTs resulted in improved mechanical properties. However,

increasing the CNT content to 1 wt.% gradually deteriorated the properties due to agglomeration. Moreover, most or all CNTs were consumed and transformed into ceramic phases during the firing process, sacrificing their intrinsic advantages. To address these issues, a SiC_xO_y coating was applied to the surface of CNTs using polycarbosilane (PCS) as the precursor. This coating protected the CNTs from oxidation and inhibited reactions with aluminum (l, g), silicon (s, g), and carbon monoxide (g), thus reducing the formation of ceramic phases at high temperatures. As a result, the refractories' mechanical properties and oxidation resistance were enhanced [80]. Additionally, the transformation of CNTs is significantly accelerated and primarily driven by SiO (g) compared to the Si antioxidant in Al_2O_3−C refractories. Liao et al. [81] investigated the phase and microstructure evolutions of CNTs in B_4C- and Si-containing Al_2O_3−C refractories. Their findings indicated that incorporating B_4C lowers the partial pressure of SiO (g) because B_4C oxidizes before Si at lower temperatures. This oxidation prevents the transformation of CNTs at 1000 °C and suspends their transformation at higher temperatures.

CNTs tend to form hard agglomerates that are difficult to separate into individual nanotubes due to their nanoscale dimensions and the strong Van der Waals forces among them. Consequently, the potential benefits of incorporating CNTs in CCRs have not been fully realized because of the challenges associated with the homogeneous dispersion of agglomerated nanotubes. To address these issues, in situ synthesis and CNT-decorated oxide methods have been employed to prepare CNT-containing refractories. CNTs can be synthesized by the catalytic pyrolysis of phenol-formaldehyde resins using transition metal catalysts under an inert atmosphere. Luo et al. [82] reported that multi-walled CNTs were obtained from Ni-catalyzed phenolic resin by increasing the pyrolysis temperature. These CNTs formed a net-like structure homogeneously distributed in the pores and on the surface of Al_2O_3 particles in the matrix. This addition significantly improved the mechanical properties, such as the cold modulus of rupture (CMOR) and flexural modulus, of the Al_2O_3−C refractory specimens. Liao et al. [83] indicated that B_4C could favor the formation of in situ CNTs from the resin binder and suppress the transformation of CNTs into SiC whiskers in Al_2O_3−C refractories at elevated temperatures. This enhanced toughness and thermal shock resistance of the CNT-containing Al_2O_3−C refractories.

In addition to alumina-based refractories, CNTs can be generated in situ in magnesia-based refractories. Wei et al. [84] reported that Fe nanosheets could catalyze phenolic resin to produce CNTs in low-carbon MgO−C refractories. Compared to specimens without the catalyst, those with the catalyst exhibited a 25% increase in CMOR and significantly greater displacement during the three-point bending test. The addition of metallic additives can reduce the partial pressures of oxidizing gases and increase that of hydrocarbon gases, thereby promoting the in situ formation of CNTs in the matrix. Zhu et al. [85] investigated the role of Al and Si additives and various heat-treatment temperatures (800–1400 °C) in the graphitization process of phenolic resin in the MgO−C refractory matrix. Their findings indicated that, compared to specimens containing Si powder, the addition of metallic Al was more conducive to the growth of straight and bamboo-like CNTs, facilitated by the catalyst.

The dispersion of CNTs in refractories significantly impacts their performance, and oxide/CNT composite powders can enhance the uniformity of CNT dispersion in the matrix. Feng et al. [86] prepared CNTs/$MgAl_2O_4$ whisker composite powders, with their microstructure and energy dispersive spectroscopy results in Figure 3a,b. The CNTs interlocked with $MgAl_2O_4$ whiskers, facilitating their uniform dispersion within the refractory matrix. Thermal shock test results showed the residual strength ratio of low-carbon Al_2O_3−C refractories containing 3.0 wt.% CNTs/$MgAl_2O_4$ was 39.2%, 97.0% higher than the blank sample (Figure 3c). The presence of CNTs and $MgAl_2O_4$ whiskers significantly improved thermal shock resistance due to mechanisms like "bridging", "crack deflection", and the generation of microcracks in the matrix. Additionally, the mechanism by which CNTs/$MgAl_2O_4$ prevented the propagation of the main crack was illustrated in Figure 3d. During the thermal shock process, crack deflection due to the presence of flake graphite with excellent sliding properties on the surface layer of the aggregates can be formed. However, this effect was insufficient to stop the main crack's propagation completely. When the crack penetrated the aggregates, multiple deflections occurred within the spinel, and a large number of microcracks formed around the area where it encountered the CNT-wrapped cubic $MgAl_2O_4$. The crack deflection increased the path of the main crack propagation, and the formation of microcracks created new surfaces. All of these induced the elastic strain energy release in the refractory, effectively inhibiting the catastrophic propagation of cracks. Furthermore, the $MgAl_2O_4$ whiskers in the matrix and other in situ formed ceramic whiskers consumed thermal stress through stretching and bridging, thus preventing crack propagation. Li et al. [87] prepared CNT/MgO composite powders using a catalytic combustion synthesis method. SEM images showed that cubic MgO particles, along with fibrous CNTs were uniformly distributed in the prepared samples, the aspect ratio of the CNTs was 200 (Figure 3e). TEM results confirmed that the prepared CNTs had a typical hollow bamboo-like structure (Figure 3f). Additionally, thermal shock test results (Figure 3g) indicated that increasing the

content of composite powder enhanced the residual strength ratio of the samples. When 2.5 wt.% of CNT/MgO composite powder was added, the residual strength ratio of the samples was 63.9% higher than that of the pristine samples.

In addition to the previously mentioned methods, chemical vapor deposition (CVD) has proven effective for generating CNTs. Liang et al. [88] first prepared Al_2O_3/MWCNT composite powders via the catalytic decomposition of methane and subsequently incorporated these powders into Al_2O_3−C refractories. This approach achieved a uniform distribution of MWCNTs within the Al_2O_3−C refractory matrix, thereby enhancing the thermal shock resistance of the refractories. Li et al. [89] synthesized nano carbon-decorated Al_2O_3 powders through CVD, using ethanol as the carbon source and Ni as the catalyst. SEM images of the samples (Figure 3h) revealed a substantial formation of MWCNTs on the surfaces of Al_2O_3 powders with minimal catalyst loading. Introducing MWCNT-decorated Al_2O_3 powder into Al_2O_3−C refractories stimulated the growth of SiC whiskers within the matrix, significantly improving thermal fracture resistance and providing residual strengths 1–2 times higher than those of original nano carbon black-containing refractories (Figure 3i). Figure 3j illustrates the toughening mechanism, where MWCNTs promoted the growth of SiC whiskers, thereby enhancing thermal fracture resistance. The "pull-out" and "bridging" mechanisms of MWCNTs and SiC whiskers explain the observed strengthening properties.

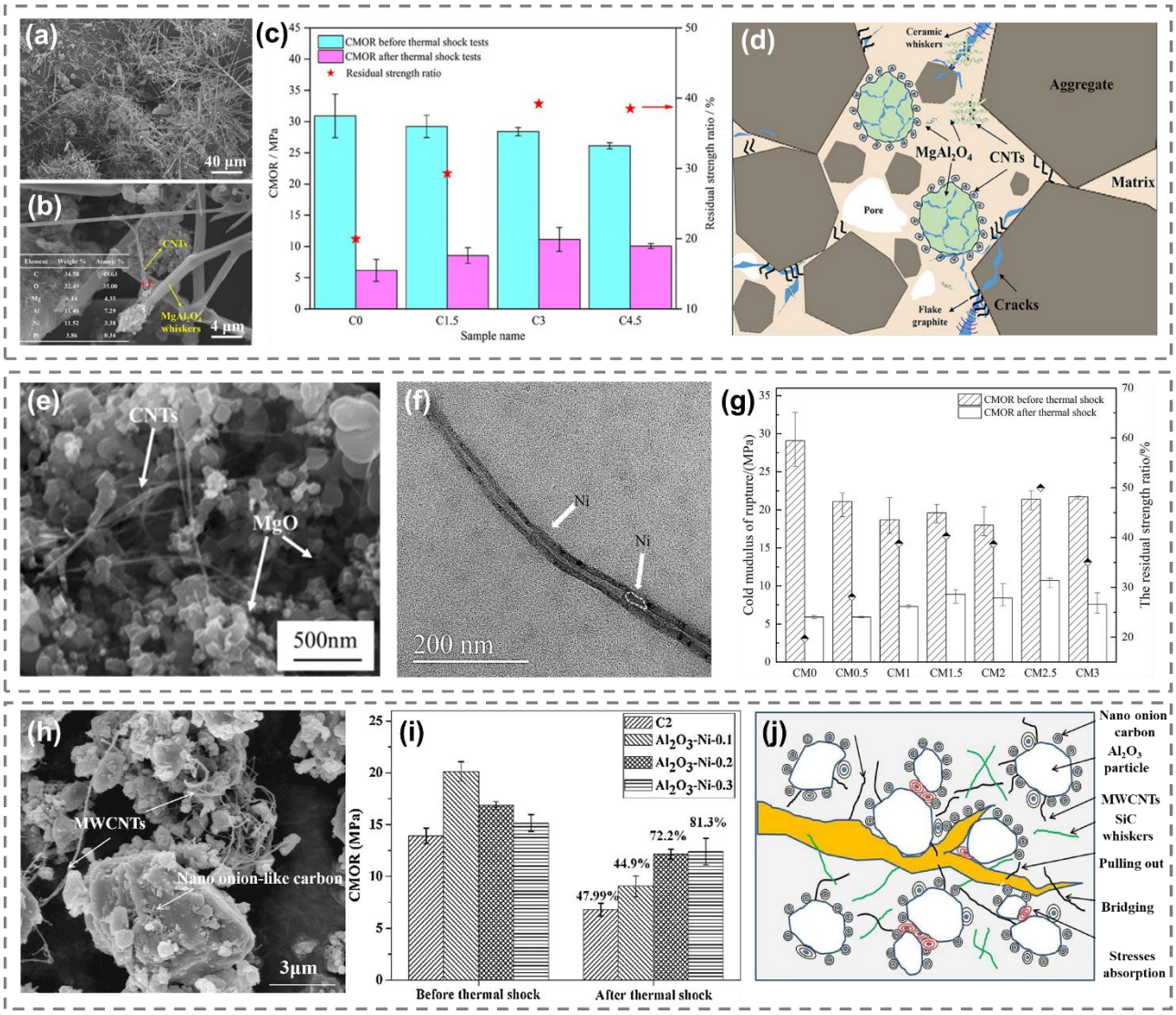

Figure 3. (**a**) SEM images and (**b**) energy dispersive spectrometry (EDS) results of the CNTs/$MgAl_2O_4$ sample. (**c**) CMOR of Al_2O_3−C refractories before and after thermal shock tests and their residual strength ratio. (**d**) Schematic diagram of crack propagation in the CNTs/$MgAl_2O_4$ sample under thermal shock [86]. (**e**) SEM image of the CNTs/MgO composite powders. (**f**) TEM image of CNTs in the CNTs/MgO sample. (**g**) CMOR and residual strength ratio of Al_2O_3−C refractory with CNTs/MgO composite powders before and after thermal shock test [87]. (**h**) SEM image of nano carbon composites@Al_2O_3 powder. (**i**) CMOR of Al_2O_3−C refractory with nano carbon composites@Al_2O_3 powder before and after thermal shock test. And (**j**) schematic diagram

of nanocomposites strengthening and toughening mechanisms in the Al_2O_3−C matrix [89]. (**a**–**d**) Copyright 2024, John Wiley and Sons; (**e**–**g**) Copyright 2022, Elsevier; (**h**–**j**) Copyright 2018, Elsevier.

2.3. Graphene Nanosheets Containing Refractories

Graphene, a two-dimensional material, has recently garnered significant attention due to its unique electronic, mechanical, and thermal properties [90–101]. These exceptional characteristics make graphene an ideal candidate for various applications, including nanoelectronics, nanocomposites, supercapacitors, and chemical/biological sensors [102–112]. Graphene nanosheets (GNSs), consisting of one or more layers of graphene, serve as an alternative reinforcement material comparable to CNTs and have demonstrated significant improvements in the service properties of CCRs.

Expanded graphite (EG), derived from graphite and featuring a long-range ordered layered structure made up of parallel graphene nanosheets, exhibits remarkable mechanical properties, including compressibility, resilience, high tensile strength, and a high elastic modulus [113–116]. Consequently, EG has been utilized as a reinforcement and carbon source in CCRs, substituting traditional graphite flakes. Behera et al. [117] used EG as a partial replacement for flake graphite in 5 wt.% graphite-containing MgO−C refractories. The composition containing 0.8 wt.% EG achieved a 20% increase in CCS and a 120% higher hot modulus of rupture (HMOR), successfully enduring 12 thermal cycles without failure. Additionally, they introduced EG into commercial Al_2O_3−C refractory slide gate plates. Using EG as a carbon source facilitated the formation of a flaw-tolerant microstructure, with in situ catalytic formation of nanostructured interconnected SiC whiskers in the matrix, which enhanced mechanical properties. Kim et al. [118] investigated the impact of varying EG content (0−4 wt.%) in MgO−C bricks with a total graphite content of 15 wt.%. They found that as the EG content increased, the fracture strength decreased, but thermal shock resistance improved due to the increase in apparent porosity, which buffered the thermal expansion of MgO. However, EG can be easily pulled out, leading to weak interfacial bonding strength, thereby limiting its reinforcement effect. To address this issue, Wang et al. [119] prepared β-SiC whiskers hybridized with EG and SiO_x spheres hybridized with EG, then introduced them into Al_2O_3−C refractories. These hybridized phases acted like "tree roots," increasing the interfacial shear strength of the refractory and absorbing fracture energy during failure. As a result, the refractories' mechanical properties and thermal shock resistance were significantly improved.

In addition, structural degradation and oxidation of graphene nanosheets often originate from unpaired carbon atoms [120–125]. Doping boron (B) or nitrogen (N) elements into graphene can improve structural stability and expand its application prospects in refractories. Wang and his team [126] effectively incorporated boron and nitrogen into the carbon framework through various C−B bonds (such as B_4C, B−sub−C, and BC_2O) and C−N bonds (including pyridine-N, amino-N, and graphitic-N). This was achieved while preserving the hexagonal graphitic structure and diminishing its reactivity. The SEM image shown in Figure 4a revealed the porous structure and graphite layers of B-doped EG. Due to its similar morphology and microstructure to EG, the doped EG could also be considered a potential reinforcement material. Compared to as-received EG, the B-doped and N-doped EG retained a relatively intact structure in Al_2O_3−C refractories at high temperatures due to fewer defects and lower reactivity. The fracture behavior of specimens incorporating B-doped and N-doped EG was shown in Figure 4b,c. At 800 °C, specimens with EG, B-doped EG, and N-doped EG demonstrated greater force and displacement values than those with 1 wt.% flake graphite, attributed to their enhancing and toughening effects. At 1200 °C, EG promoted the formation of numerous β-SiC whiskers, while B-doped and N-doped EG mitigated performance decline due to EG's structural changes. Therefore, at 1200 °C, the synergistic effects of B/N-doped EG and the in situ generated β-SiC whiskers enhanced the fracture properties of the refractory material. Additionally, the relatively intact structure of B-doped and N-doped EG at 1200 °C indicated more efficient thermal stress absorption and release. Consequently, specimens containing B-doped EG and N-doped EG exhibited the highest residual strength ratios (Figure 4d). In the oxidation resistance test (Figure 4e), the B/N-doped EG showed less weight change than EG, indicating enhanced oxidation resistance.

Graphene nanosheets (GNSs) have high mechanical strength and thermal conductivity [127–132]. Compared with EG, GNSs possess a higher specific surface area, and the volume effect of GNSs effectively enhances the mechanical, thermal, and electrical properties of ceramic matrix composites [133–138]. GNSs can be prepared by three techniques: (i) mechanical exfoliation, (ii) epitaxial growth, and (iii) graphene oxide reduction [139–146]. Among these methods, the mechanical exfoliation technique is particularly notable for its simplicity, low cost, and high efficiency, making it one of the most promising approaches for producing GNSs. GNSs/MgO and GNSs/Al_2O_3 composite powders can be obtained by ball-milling EG and oxide powders. This process ensures a uniform distribution of GNSs in alumina and

magnesia powders, with the thickness and size of GNSs dependent on the amount of EG added. The incorporation of GNSs composite powders enhances the mechanical properties and thermal shock resistance of CCRs. In the magnesia−carbon system, the highly reactive GNSs can reduce the partial pressure of oxygen, increasing the partial pressure of N_2 gas. This promotes the formation of more AlN ceramic phases within the matrix, thereby strengthening and toughening the MgO−C refractories [147]. In the alumina−carbon system, GNSs can improve mechanical properties by stimulating the growth of SiC whiskers at lower temperatures, owing to their higher reactivity compared to graphite.

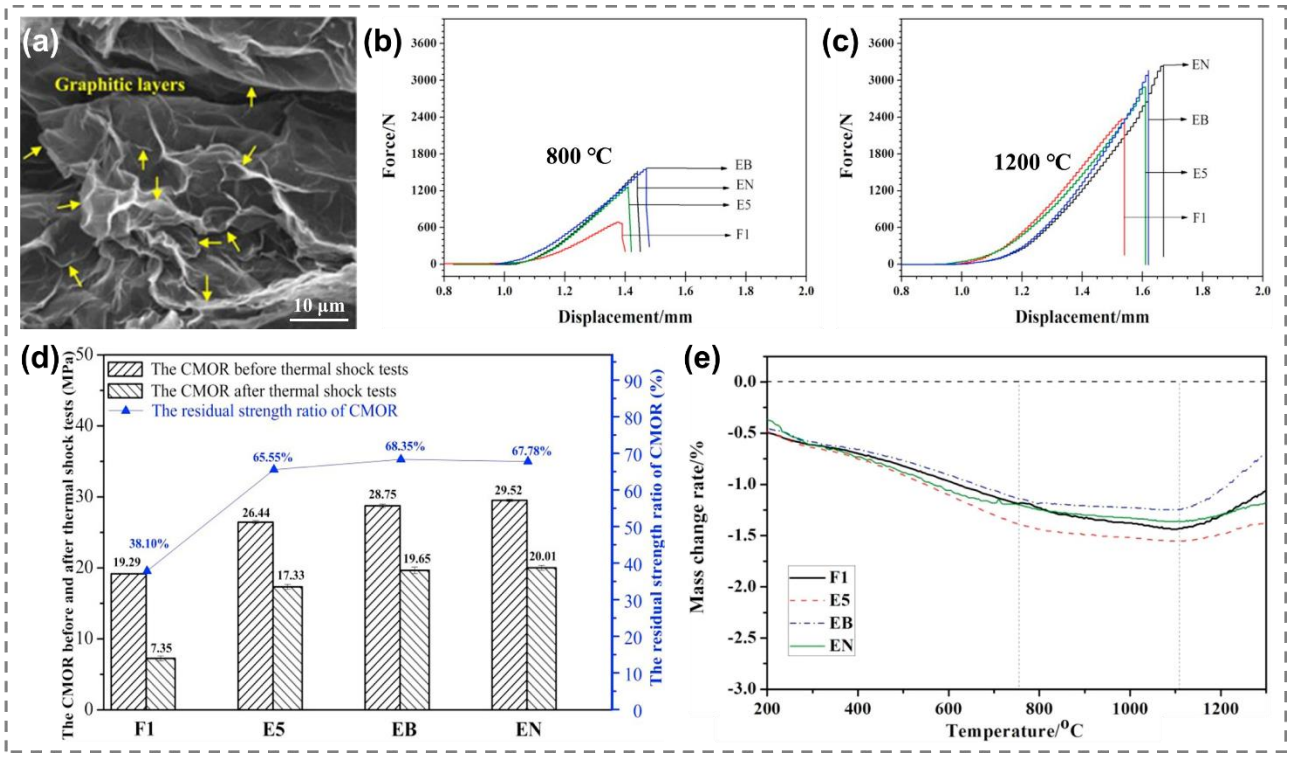

Figure 4. (**a**) SEM micrographs of B-doped EG. Force−displacement curves of the specimens fired at (**b**) 800 °C and (**c**) 1200 °C. (**d**) Residual CMOR and the residual strength ratio of CMOR of the specimens fired at 1200 °C after 5 thermal shock cycles. And (**e**) mass change of the specimens fired from room temperature to 1300 °C in air [126]. (**a**–**e**) Copyright 2017, Elsevier.

To achieve the homogeneous distribution of GNSs several nanocomposite powders were prepared and then used in Al_2O_3−C and MgO−C refractories. Ding et al. [148] developed multilayer graphene/$MgAl_2O_4$ composite powders using a one-step carbon-bed sintering process, with magnesium citrate serving as the source for both MgO and carbon. The resulting products contained 5.96 wt.% carbon, with graphene layers (6–10 layers) located between or outside the $MgAl_2O_4$ grains. These C/$MgAl_2O_4$ composite powders absorb strain energy and thermal stress, forming short fibrous ceramic phases within the matrix. As a result, incorporating C/$MgAl_2O_4$ composite powders significantly enhanced the thermal shock resistance of low-carbon Al_2O_3−C refractories. Lv et al. [149] successfully synthesized GNSs using a liquid-phase shear exfoliation method. To enhance their properties, they modified the surface of these GNSs with AlOOH nanofibers before incorporating them into MgO-based castables, as illustrated in Figure 5a. The characterization of the GNSs using TEM and AFM techniques revealed that the nanosheets had an exceptionally thin structure, comprising approximately 10 atomic layers (Figure 5b,c). Moreover, a digital photograph (Figure 5d) demonstrated the excellent stability of the GNSs suspension, which remained uniformly dispersed in solution over an extended period, indicating the high quality of the exfoliated nanosheets. Following hydrothermal treatment, the fibrous AlOOH was uniformly integrated with the GNSs, as confirmed by TEM imaging (Figure 5e). This modification significantly enhanced the water wettability of the GNSs, facilitating their uniform dispersion within the castable material. The improved dispersion contributed to enhanced thermal shock resistance of the castables. Notably, the incorporation of 0.5 wt.% GNSs into the castables resulted in a 17% increase in the residual strength ratio compared to the pristine samples (Figure 5f), demonstrating the effectiveness of the surface modification and the potential of GNSs as a reinforcement material in refractory applications. Furthermore, Liu et al. [150] used a three-roll mill method to exfoliate flake graphite in a phenolic resin (PF) medium for the synthesis of the GNSs/PF composite, which were then introduced into MgO−C bricks (Figure 6a). A mathematical model was established to show the relationship between graphite flake thickness and the number of exfoliation cycles (the inset of Figure 6a), indicating that satisfactory

thickness was achieved after approximately 16 exfoliation cycles. The SEM image (Figure 6b) confirmed that the thickness ranged between 8.59–18.26 nm, and the TEM image (Figure 6c) further verified this result. Comparative tests were conducted on refractory samples with 8 wt.% flake graphite (sample S1) and those with the GNSs/PF composite (carbon content approximately 2 wt.%). The results showed that samples with the composite exhibited superior high-temperature flexural strength (Figure 6d) and oxidation resistance (Figure 6e) despite having lower carbon content.

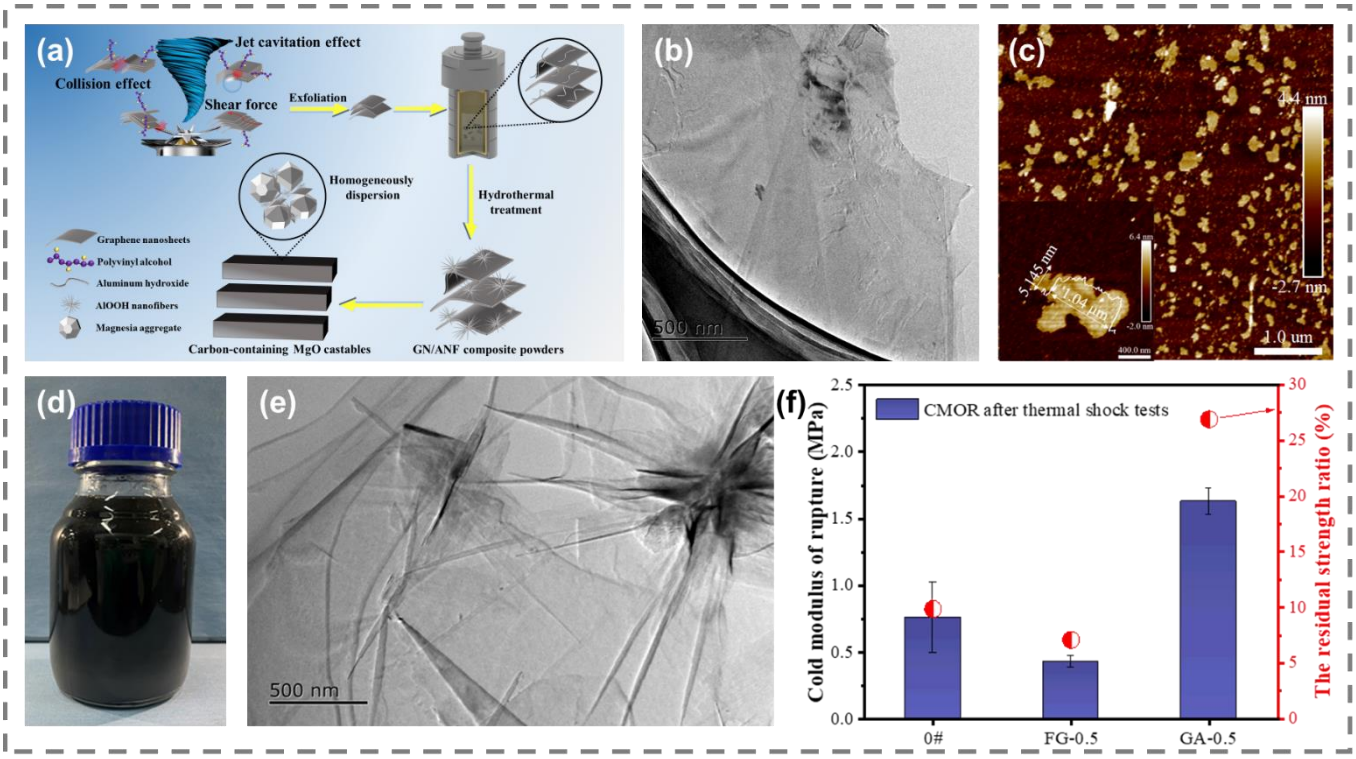

Figure 5. (**a**) Schematic diagram of liquid-phase shear exfoliation process and the preparation of carbon-containing MgO castables. (**b**) TEM and (**c**) AFM images of GNSs exfoliated by kitchen blender under the optimal processing parameters. (**d**) Digital photographs of GNSs suspension after 15 days of resting. (**e**) TEM image of GNSs/AlOOH composite powders prepared at the optimal conditions (190 °C and pH = 3). (**f**) HMOR values of castable samples measured at 1400 °C for 30 min. And (**e**) CMOR and residual strength ratios of castable specimens after three thermal shock cycles at 1100 °C [149]. (**a**–**f**) Copyright 2024, Elsevier.

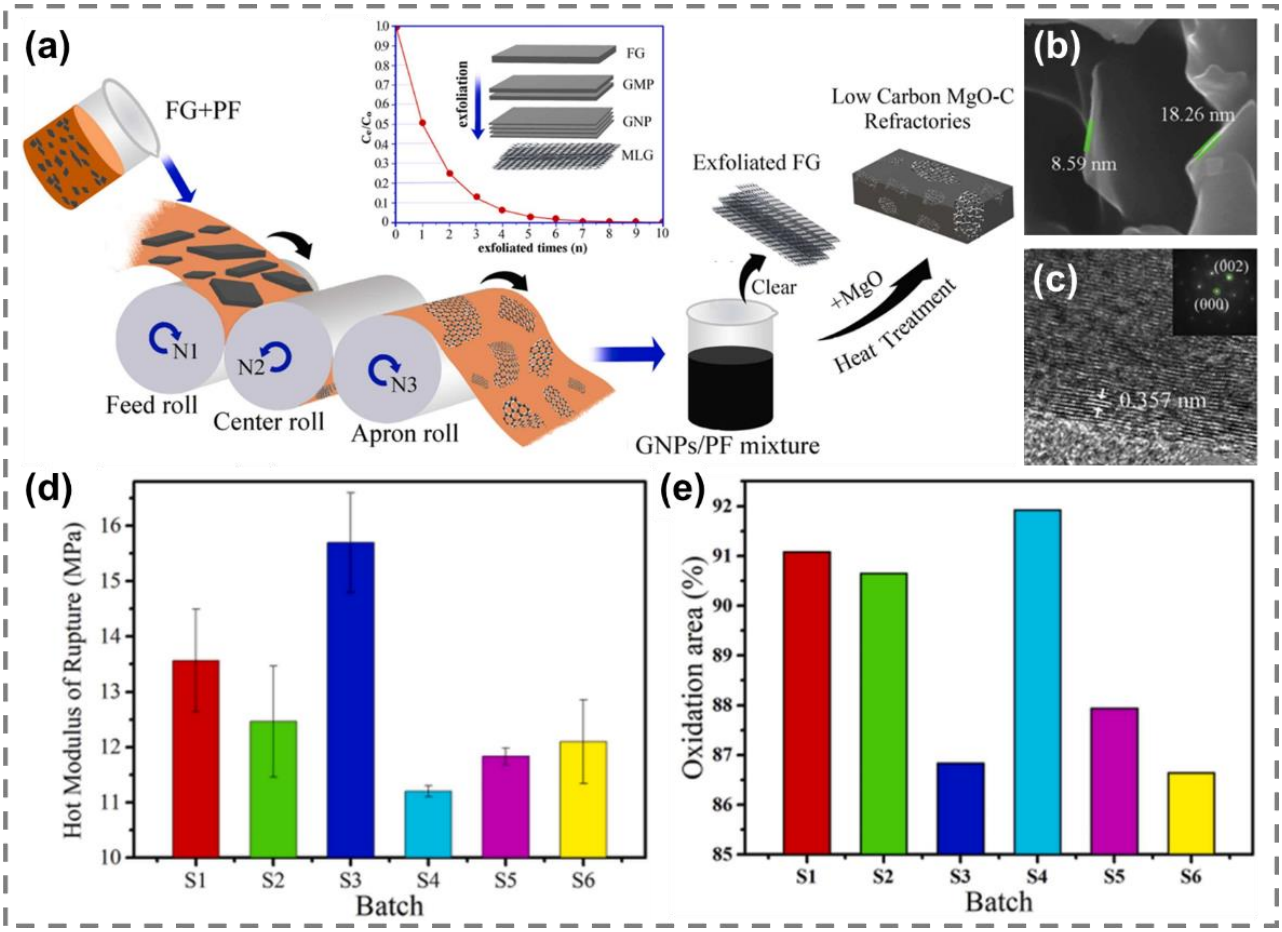

Figure 6. (**a**) Preparation for GNSs or GNSs/PF mixture from flake graphite in PF and further obtain low carbon MgO−C refractories, and mathematical model drawing the results of exfoliating flake graphite. (**b**) SEM images of the horizontal and vertical morphologies of products with 10 wt. % flake graphite exfoliated from flake graphite in PF with three-roll milling for 16 cycles. (**c**) HRTEM image of the GNSs with diffraction pattern (inset). (**d**) HMOR of the prepared MgO−C bricks after heat-treatment at 1350 °C for 0.5 h. And (**e**) percentage oxidation area of MgO−C bricks after 1h oxidation at 1400 °C [150]. (**a**–**e**) Copyright 2023, Elsevier.

In summary, introducing nanocarbon can significantly improve the mechanical properties and thermal shock resistance of CCRs. However, the application of nanocarbon materials also faces several shortcomings: (1) Direct addition tends to cause agglomeration, making it difficult to disperse uniformly in the matrix. (2) The structural collapse of nanocarbon materials often occurs due to reactions between carbon and anti-oxide vapors (Al (g), Si (g), and SiO (g)) at high coking temperatures. And (3) the preparation of graphene composite powder by mechanical exfoliation has a low yield, complex process, and high cost, which makes it challenging to implement in practical production applications. Therefore, to further enhance the reinforcement effect of nanocarbon materials, it is imperative to explore new methods to improve their structural stability and minimize related interfacial reactions. Table 1 provides a summary of the application of nanocarbons in CCRs and their associated properties.

Table 1. Summary of the application of nanocarbons in CCRs and their effects on the properties.

Classification	Refractory Type	Methodology	Novel Carbon Content (wt.%)	Flake Graphite Content (wt.%)	Refractory Property Improvement	Mechanism	Ref.
Carbon black	Al_2O_3−C refractories	Direct addition	0.5~2.5 (N220, N990)	8	Mechanical properties, oxidation resistance, slag corrosion resistance	High surface area of nanocarbon, strengthening effect of in situ ceramic phases	[55]
	MgO−C refractories	Direct addition	0~1.5	3–5	Densification, strength, corrosion resistance	Filling effect, nano carbon absorbs and relieves the stress	[59]
	MgO−C refractories	Direct addition	1 (N220)	5	Mechanical properties, oxidation resistance, slag corrosion resistance	Filling effect, strengthening effect of in situ formed ceramic phases	[70]
	Al_2O_3−C refractories	Ball milling dispersion	1 (N220)	3	Mechanical performances, thermal shock resistance	Strengthening effect of in situ formed MWCNTs and SiC whiskers	[58]
	Al_2O_3−C refractories	Ball milling dispersion	0.5~1 (N220)	5	Mechanical properties, thermal shock resistance	Thermal stress absorption effect of nano carbon black, strengthening effect of SiC whiskers	[57]
Carbon nanotubes	MgO−C refractories	Direct addition	0.18	2	Bulk density, oxidation resistance, slag corrosion resistance	Effective surface area, filling effect	[78]
	Al_2O_3−C refractories	CNTs/$MgAl_2O_4$ whiskers composite	1.5–4.5 (composite powders)	2	Thermal shock resistance	"Bridging" and "crack deflection" by CNTs and $MgAl_2O_4$ whiskers, generation of microcracks	[86]
	Al_2O_3−C refractories	CNTs/MgO composite powders	0.5–3 (composite powders)	2	Thermal shock resistance	Improvement of bending crack propagation path from aggregate to matrix	[87]
	MgO−C refractories	In situ catalytic formation	–	3	High-temperature mechanical properties	Releasing of the residual intrinsic stress and the microcrack healing	[151]
	Al_2O_3−C refractories	Nano carbon decorated oxide powders	–	1	Mechanical properties, thermal shock resistance	"Pulling out" and "bridging" mechanisms, energy dissipation mechanisms	[89]
Graphene nanosheets	MgO−C refractories	Liquid-phase shear exfoliation and hydrothermal process	0.25, 0.5	1	Mechanical properties, thermal shock resistance	Homogeneous distribution of GNSs, even distribution of thermal stress	[149]
	MgO−C refractories	Three-roll milling in phenolic resin	0.3, 0.56	2	Mechanical properties, oxidation resistance, slag corrosion resistance	GNSs continue uniformly dispersed and wrapped with refractories aggregate	[150]
	Al_2O_3−C refractories	C/$MgAl_2O_4$ composite powders	1.5–6 (composite powders)	2	Thermal shock resistance, oxidation resistance, slag corrosion resistance	"Bridging" mechanisms of in situ short fibrous ceramic phases	[148]
	Al_2O_3−C refractories	Ball milling dispersion	0.5	0.5	Mechanical properties, thermal shock and oxidation resistance	Effective thermal stress absorption and release mechanism	[126]

3. Nano Non-Oxides Containing Refractories

Non-oxide ceramic phases, such as nitrides, carbides, and MAX phases, considerably improve the slag corrosion resistance, oxidation resistance, and thermomechanical properties of CCRs [152–163]. Hexagonal boron nitride (h-BN), which shares a structure similar to graphite, is widely utilized as a reinforcement agent in CCR composites because of its outstanding thermal stability and oxidation resistance [164–168].

Liang et al. [166] substituted alumina fine powder with h-BN in refractory preparation, investigating how varying h-BN content and heat treatment temperature impacted the samples' physical properties and thermal shock resistance. The findings revealed that with an increase in h-BN content, the mechanical properties of the refractory diminished due to h-BN's chemical inertness, which hindered composite sintering. Nevertheless, thermal shock tests indicated that the sample containing 20 wt.% h-BN exhibited the optimal thermal shock resistance attributed to the weak-bonding interface between h-BN and the matrix. Ji et al. [169] explored the effects of commercial h-BN sheet content and particle size on the comprehensive properties of low-carbon Al_2O_3−C refractories. They found that adding h-BN decreased the diameter of SiC whiskers, thereby enhancing their strengthening effect and improving resistance to crack propagation, oxidation, and thermal shock. The best overall properties were achieved with the addition of 0.5 wt.% h-BN sheets. The size of h-BN significantly influenced the mechanical properties: larger-sized h-BN (1–10 μm) improved flexural strength, whereas smaller-sized h-BN (~0.1 μm) enhanced thermal shock resistance. Zheng et al. [170] prepared h-BN composite powders using a magnesiothermic reduction combustion synthesis route and incorporated them into low-carbon Al_2O_3−C refractories. The introduction of h-BN resulted in the in situ formation of spinel and AlN whiskers, leading to crack deflection and branching into finer cracks. When 1.0 wt.% h-BN composite powders were added, the refractories exhibited the highest residual strength retention (~35%). Besides h-BN's chemical inertness, the in situ formation of spinel and AlN whiskers, coupled with reduced pore size, significantly enhanced slag corrosion resistance. As the composite powder addition increased from 0 to 2 wt.%, the slag corrosion index dropped from 19.74% to 8.15%. Moreover, Fan et al. [171] addressed the challenge of reduced oxidation and thermal shock resistance in low-carbon MgO−C refractories by enhancing them with nano-layered BN-modified graphite prepared using a molten salt method. Their findings indicated that incorporating 1–4 wt.% of this modified graphite improved the mechanical properties of MgO−C refractories. This improvement was due to enhanced bonding between the matrix and in situ generated rod-like Mg_2SiO_4, columnar $MgAl_2O_4$, and $Mg_3B_2O_6$ liquid phases, which filled the pores and increased strength. Additionally, the oxidation index of MgO−C refractories with 4 wt.% nano-layered BN-modified graphite decreased by 34% compared to unmodified samples. This enhancement was attributed to the filling effect of in situ generated Mg_2SiO_4 and the protective layer formation of $Mg_3B_2O_6$ derived from BN oxidation.

Compared to traditional h-BN nanosheets, rod-like h-BN is better suited for applications requiring high thermal conductivity, high strength and high-temperature stability. Li et al. [172] synthesized rod-like h-BN composed of numerous small nanosheets through a precursor catalytic pyrolysis process and used it to create a novel rod-like h-BN modified low-carbon Al_2O_3−C refractory. The SEM image (Figure 7a) revealed that the synthesized h-BN had a rod-like morphology with uniform size distribution and an average diameter of approximately 2 μm. The TEM image showed that the rod-like h-BN consisted of many small nanosheets (Figure 7b), and HRTEM results displayed a layered structure with clear lattice fringes and an interplanar spacing of about 0.345 nm, corresponding to the (002) plane of h-BN (Figure 7c). Furthermore, adding rod-like h-BN significantly increased the high-temperature slag-wetting angle of the refractory. As depicted in Figure 7d–f, the contact angle of the sample with 3 wt.% flake graphite gradually decreased to 27.6° within 720 seconds. However, replacing just 1 wt.% flake graphite with rod-like h-BN resulted in a contact angle decrease to only 55.8° over the same period. Figure 7g showed the change in slag height over time, indicating that as the slag spread on the sample surface, the height decreased, and the contact angle followed a similar trend. These results demonstrated that the addition of rod-like h-BN improved the slag penetration resistance of the refractory.

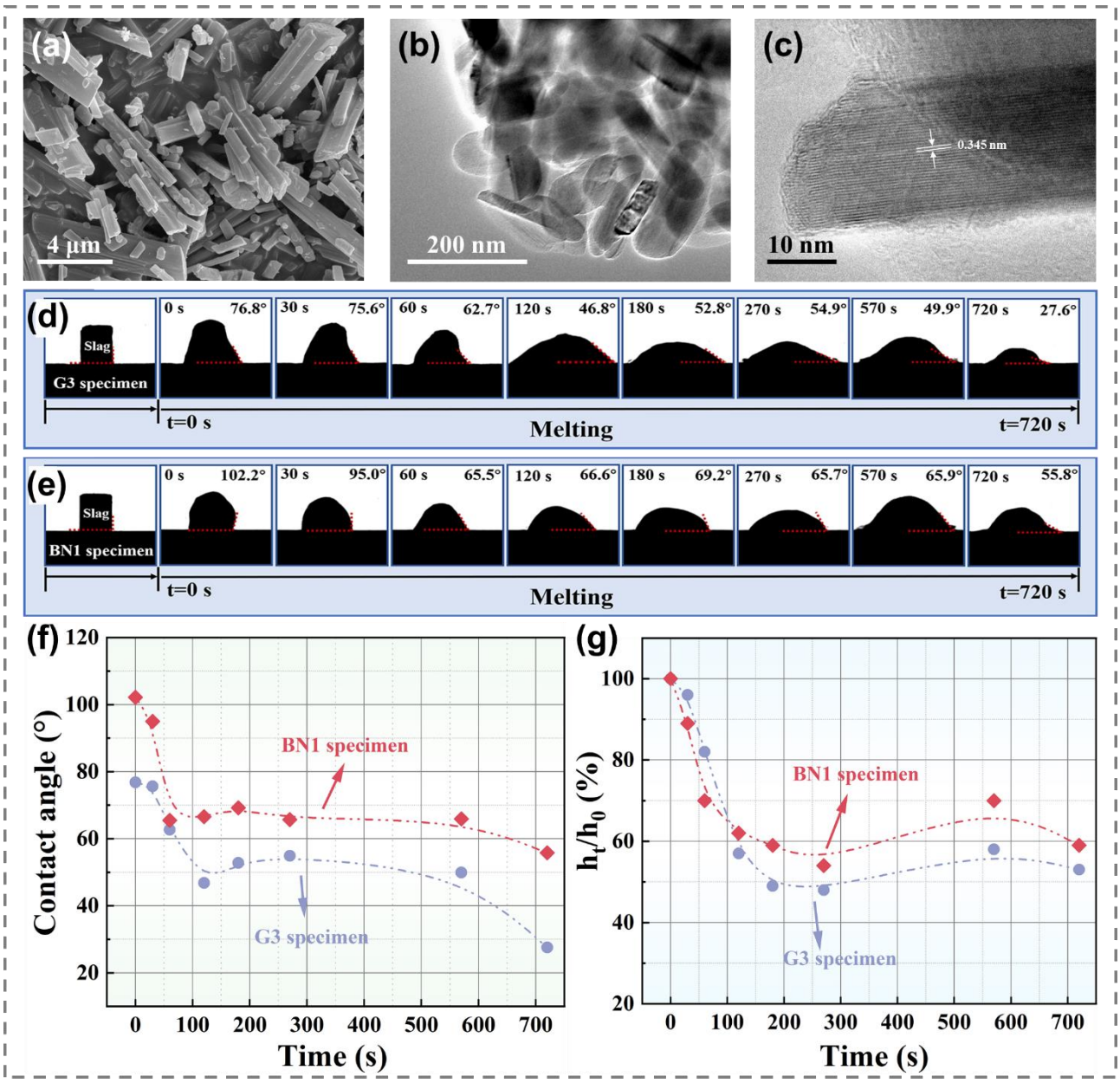

Figure 7. (**a**) SEM image, (**b**) TEM image, and (**c**) HRTEM image of the as-synthesized h-BN sample fired at 1200 °C. Evolution of the molten slag wetting process on the surface of sample G3 with (**d**) 3 wt.% flake graphite and sample BN1 with (**e**) 2 wt.% flake graphite and 1 wt.% rod-like h-BN. And (**f**) evolution of the contact angle and (**g**) the apparent height of the molten slag on the surface of sample G3 and sample BN1 [172]. (**a**–**g**) Copyright 2024, Elsevier.

SiC nanowhiskers (SiC_w) are known for their high melting point, excellent corrosion resistance, and chemical stability. Chen et al. [173] investigated the effects of different carbon sources on lightweight Al_2O_3−C refractories containing silicon additives. They found that samples using highly reactive microcrystalline graphite produced more SiC_w in the microporous corundum aggregates compared to those using flake graphite. The increased SiC_w content resulted in a denser and more interwoven microporous aggregate/matrix interface structure, enhancing the performance of the refractories. This confirmed that utilizing highly reactive graphite along with silicon-containing antioxidant powders can significantly improve the mechanical properties of Al_2O_3−C refractories. Zhen et al. [174] developed an in situ growth method for SiC_w by adding catalysts to enhance the performance of MgO−Al_2O_3−C (MAC) refractories. Their results showed that adding 0.8 wt.% $Ni(NO_3)_2$ catalyst led to the highest performance, with CCS and CMOR values of 56.50 MPa and 10.52 MPa, respectively. The thermal shock and oxidation resistance of MAC refractories were also enhanced through crack deflection and bridging mechanisms induced by SiC_w. Chen et al. [175] successfully synthesized SiC_w using rice husk powders and attempted to reduce the flake graphite content in refractories by adding the synthesized SiC_w. The results indicated that the addition of SiC_w significantly affected the microstructure and mechanical properties of MgO−C refractories with different graphite contents. Introducing SiC_w promoted the generation and growth of ceramic phases in MgO−C refractories. The addition of 1 wt.% SiC_w allowed for a reduction

of 1 wt.% graphite content. Furthermore, the synergistic effect of the introduced SiC_w and the generated ceramic phases improved the thermal shock resistance and oxidation resistance of the refractories.

In addition to the in situ growth and direct addition of SiC_w in refractories, forming composite powders with SiC whiskers and other materials also enhances refractory performances. Li et al. [176] synthesized SiC nanofiber-coated graphite flakes at a relatively low temperature of 1623 K through an in situ catalytic reaction using $Co(NO_3)_2{\cdot}6H_2O$ as the catalyst precursor. Al_2O_3−C castables incorporating these SiC nanofiber-coated graphite flakes exhibited a 73.1% higher residual CMOR ratio after thermal shock testing, 20.0% lower oxidation, and 43.5% less slag corrosion compared to reference samples with pristine graphite. Liu et al. [177] produced graphite-SiC_w composite powders using a salt-assisted synthesis method involving Si powders, graphite, and a molten salt medium. SiC whiskers, measuring 10–50 nm in length, formed on the surface of the flake graphite, increasing the oxidation activation energy of the graphite−SiC_w composite powder. The SiC cladding layer reacted with slag at high temperatures, enhancing the viscosity of the liquid, thus providing the samples with improved oxidation and slag resistance. Similarly, Ban et al. [178] synthesized ZrB_2−SiC_w composite powders using a microwave-assisted carbo/borothermal reduction method. SEM images and EDS results of the as-prepared samples (Figure 8a) revealed that the SiC_w were very fine and uniformly distributed with ZrB_2. As shown in Figure 8b, the residual CMOR slightly increased with the addition of ZrB_2−SiC_w composite powders after the thermal shock test, maintaining high residual strength ratios of 65% to 85%. This improvement was primarily due to the low thermal expansion coefficient and good thermal conductivity of ZrB_2−SiC_w. The slag corrosion test setup is illustrated in Figure 8c, and the post-test sample photos are shown in Figure 8d. The lower half of the sample in Figure 8d indicated that the oxidation layer of the sample with 6 wt.% ZrB_2−SiC_w was thinner (1.8 mm) compared to the pristine sample (2.5 mm), demonstrating that adding ZrB_2−SiC_w composite powders significantly enhanced the corrosion and oxidation resistance of the refractories.

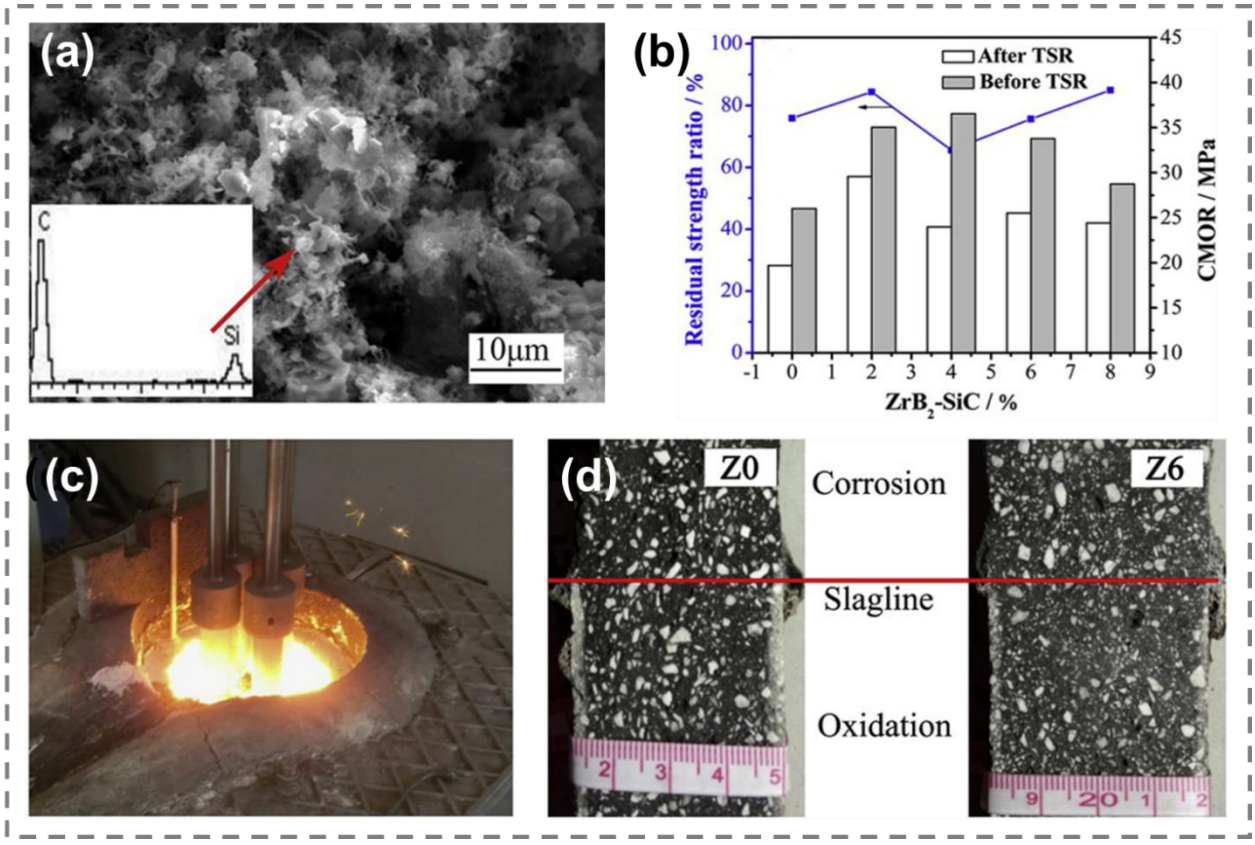

Figure 8. (**a**) Microscopic morphology of the prepared ZrB_2−SiC_w composite powder. (**b**) Residual strength ratio and CMOR of samples after thermal shock test (**c**) The corrosion testing equipment. And (**d**) cross−section of samples after corrosion test [178]. (**a**–**d**) Copyright 2020, Elsevier.

As a new type of nanomaterial, ternary non-oxides can also enhance the performances of Al_2O_3−C refractories. These additives, instead of metal additives, are preferred due to their high elastic modulus, thermal conductivity, excellent thermal shock resistance, and damage tolerance. Liu et al. [179] replaced Al with Ti_3AlC_2 to prepare low-carbon Al_2O_3−C refractories. SEM images showed the presence of Ti_3AlC_2, SiC_w, and metastable $Ti_3Al_{1-x}C_2$ formed by the selective oxidation of Ti_3AlC_2 in the refractory matrix. The SEM and EDS results (Figure 9a–c) confirmed the

presence of Ti_3AlC_2 in the inner part, with a significant reduction of Al in the outer regions, suggesting the forming of $Ti_3Al_{1-x}C_2$. Load−displacement curves of samples coked at different temperatures were shown in Figure 9d. The displacement of samples with Al was much greater at 800 °C and 1200 °C compared to the samples, which showed greater displacement after firing at 1600 °C. This was attributed to the volume expansion of Ti_3AlC_2 during oxidation, forming a dense structure that improved the mechanical properties of Al_2O_3−C refractories. Additionally, the Ti_3AlC_2-added samples demonstrated better oxidation resistance compared to the samples with Al powders (Figure 9e,f). Chen et al. [180] introduced Cr_2AlC powder into Al_2O_3−C refractories and investigated its effect on corrosion resistance. The cross-section of the samples with different Cr_2AlC contents after a crucible corrosion test at 1600 °C is shown in Figure 9g. The primary corrosion areas were at the slag/refractory interface and the slag/refractory/air interface. Calculation results of the slag penetration area revealed that Cr_2AlC addition reduced the penetration index from 32.61% to 19.34%. This improvement was attributed to the dissolution of Al_2O_3 and Cr_2O_3 from the original Cr_2AlC, which increased the local slag viscosity and suppressed further slag penetration into the refractory. Moreover, the HMOR of the Al_2O_3−C sample with 5 wt.% Cr_2AlC increased from 3.14 MPa to 5.15 MPa. Yu et al. [25] achieved the in situ generation of flake Al_4O_4C and multi-walled carbon nanotubes in Al_2O_3−C refractories by introducing Al_4SiC_4. This ternary non-oxide, known for its exceptional stability, facilitated the development of ceramic phases. Lou et al. [181] synthesized nano-$MgSiN_2$ using a molten salt method and then prepared Al_2O_3−C refractories with $MgSiN_2$ as an additive. At 1500 °C, nano-$MgSiN_2$ underwent phase reconfiguration to form Mg(g) and Si_3N_4(s), enhancing the interfacial bonding strength between aggregates and the matrix. As a result, the refractories' mechanical properties and thermal shock resistance were significantly improved.

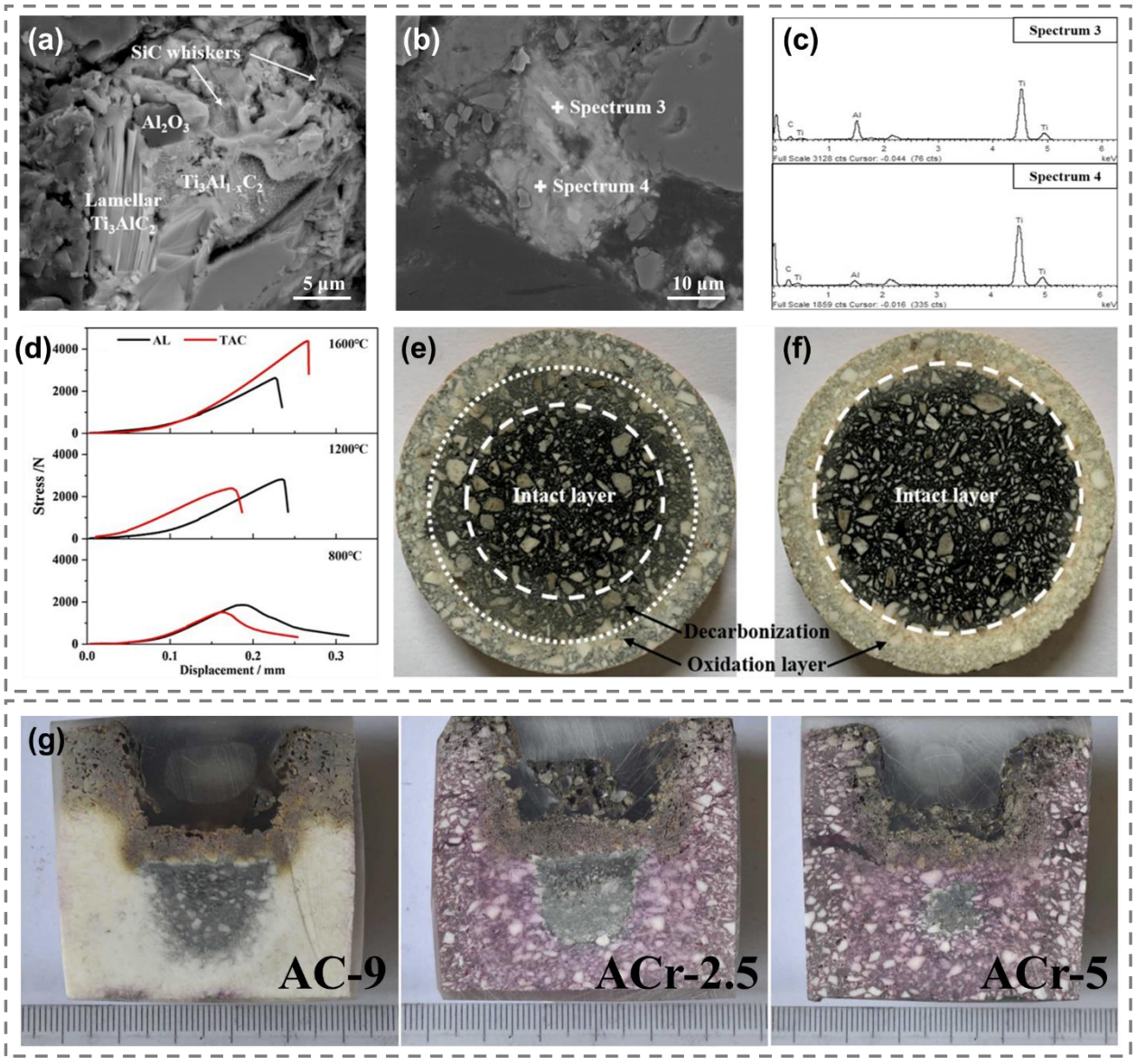

Figure 9. (**a**,**b**) SEM images of Al_2O_3−C samples with Ti_3AlC_2. (**c**) EDS spectra of the points in (**b**). (**d**) Load−displacement curves of Al_2O_3−C samples fired at different temperatures. Optical photographs of Al_2O_3−C samples with (**e**) aluminum powder and (**f**) Ti_3AlC_2 after oxidation test at 1400 °C for 0.5 h [179]. And (**g**) cross-section images of the samples with different Cr_2AlC contents after the corrosion test at 1600 °C (AC−9: 9 wt.% graphite, ACr−2.5: 6.5 wt.% graphite and 2.5 wt.% Cr_2AlC, and ACr−5: 4 wt.% graphite and 5 wt.% Cr_2AlC) [180]. (**a**–**f**) Copyright 2024, Elsevier; (**g**) Copyright 2021, Elsevier

Nano non-oxides have excellent thermal stability and corrosion resistance, showing potential for improving oxidation resistance and slag corrosion resistance of CCRs. However, nitrides and carbides have low toughness and are prone to cause brittle fracture [182–188]. The in situ formation of nitrides and carbides requires high heat-treatment temperatures and proper oxygen partial pressure, leading to the massive escape of vapors, which can result in structural degradation and strength loss of CCRs. The stability of the MAX phase at elevated temperatures is poor, and its structure usually collapses due to the phase transformation. Thus, future studies should focus on addressing these inadequacies to enhance the performances of CCRs containing nano non−oxides.

4. Nano Oxides Containing Refractories

Oxides play a crucial role in manufacturing metallic materials, petrochemical equipment, wear-resistant machinery, and other applications within the metallurgical industry [189–195]. Notably, oxides such as alumina (Al_2O_3), magnesia (MgO), spinel ($MgAl_2O_4$), and zirconia (ZrO_2) are highly valued for their exceptional resistance to extreme environments, molten steel, and slags [196–201]. These materials are integral in these industries due to their durability and stability under harsh conditions, making them indispensable in settings where high temperature and corrosive materials are constantly challenging.

Roungos and Aneziris [202] explored the integration of Al_2O_3 sheets with carbon nanotubes (CNTs) in Al_2O_3−C refractories, finding that this combination of nanoscale powders led to enhanced thermal shock performance. The dual incorporation leveraged the mechanical strength of CNTs and the thermal stability of Al_2O_3 to improve the refractory's resilience against rapid temperature changes. Ghasemi-Kahrizsangi et al. [203] observed that the addition of nano Al_2O_3 helped to fill the intergranular voids between MgO and graphite particles, thus promoting the densification of MgO−C refractories. They noted that the formation of new phases such as $MgAl_2O_4$, AlN, and Al_4C_3 in samples with 6 wt.% of both nano and micro Al_2O_3 particles enhanced the cold crushing strength (CCS), oxidation resistance, and slag resistance of these refractories. Moreover, samples containing nano-Al_2O_3 exhibited superior properties attributed to the intrinsic characteristics of Al_2O_3 nanoparticles, including significant surface effects, size effects and higher activity. Luo et al. [82] and Zhu et al. [204] developed low-carbon MgO−C refractories by incorporating a Ni-containing catalytic precursor and Al powders, leading to the in situ formation of MgO whiskers. A droplet containing Ni at the tips of some MgO whiskers suggested that the vapor−liquid−solid process controlled the growth of these whiskers. The reinforcement from these in situ formed MgO whiskers enhanced the mechanical properties of the samples with the catalyst, resulting in higher CMOR values and significantly greater displacement compared to samples without the Ni catalyst. Das et al. [205] investigated the impact of adding nanocrystalline $MgAl_2O_4$ spinel to MgO−C refractories. Their findings revealed that incorporating nano-$MgAl_2O_4$ spinel in MgO−C bricks improved physical and chemical properties, underscoring the potential for applications in the steel and refractory industries. This improvement was likely due to the spinel's ability to enhance the refractory's structural integrity and chemical stability under high temperatures.

Gu et al. [206] synthesized MgO-based aggregates with in situ formation of nanoscale $MgAl_2O_4$ grains at the boundaries and on the surfaces of MgO grains, as shown in Figure 10a. The study detailed in Figure 10b demonstrated that with the inclusion of nanoscale Al_2O_3 powders ranging from 0 to 20 wt.%, the CCS initially increased from 102.5 MPa to a peak of 302.7 MPa before decreasing to 260.3 MPa. This trend suggests that the optimal in situ formation of $MgAl_2O_4$ in MgO-based aggregates significantly enhanced their strength. Additionally, the residual strength of samples after thermal shock tests followed a similar pattern to the CCS, confirming that the appropriate formation of $MgAl_2O_4$ enhanced thermal shock resistance, as illustrated in Figure 10c. This improvement is attributed to the thermal mismatch between $MgAl_2O_4$ and MgO, which likely caused microcracks that released residual stress, thereby arresting stress around the main crack tip (shown in Figure 10e). Consequently, the introduction of nanoscale $MgAl_2O_4$ improved the physical properties and the thermal shock resistance of MgO−C refractories. Furthermore, Gu et al. [207] developed modified MgO aggregates using a nano-ZrO_2-alcohol suspension and a vacuum impregnation method, resulting in aggregates with excellent thermal shock resistance. The integration of these modified aggregates significantly bolstered the thermal shock resistance of MgO−C refractories. This enhancement is primarily attributed to the pinning effect of particles and the phase transformation toughening effect of nano-ZrO_2. Moreover, nano-ZrO_2 particles facilitated the

sintering of the matrix and the formation of the AlN ceramic phase, further improved the HMOR of the refractories. This comprehensive approach underscores the importance of material engineering at the nanoscale to enhance the performance characteristics of refractory materials in high-temperature applications.

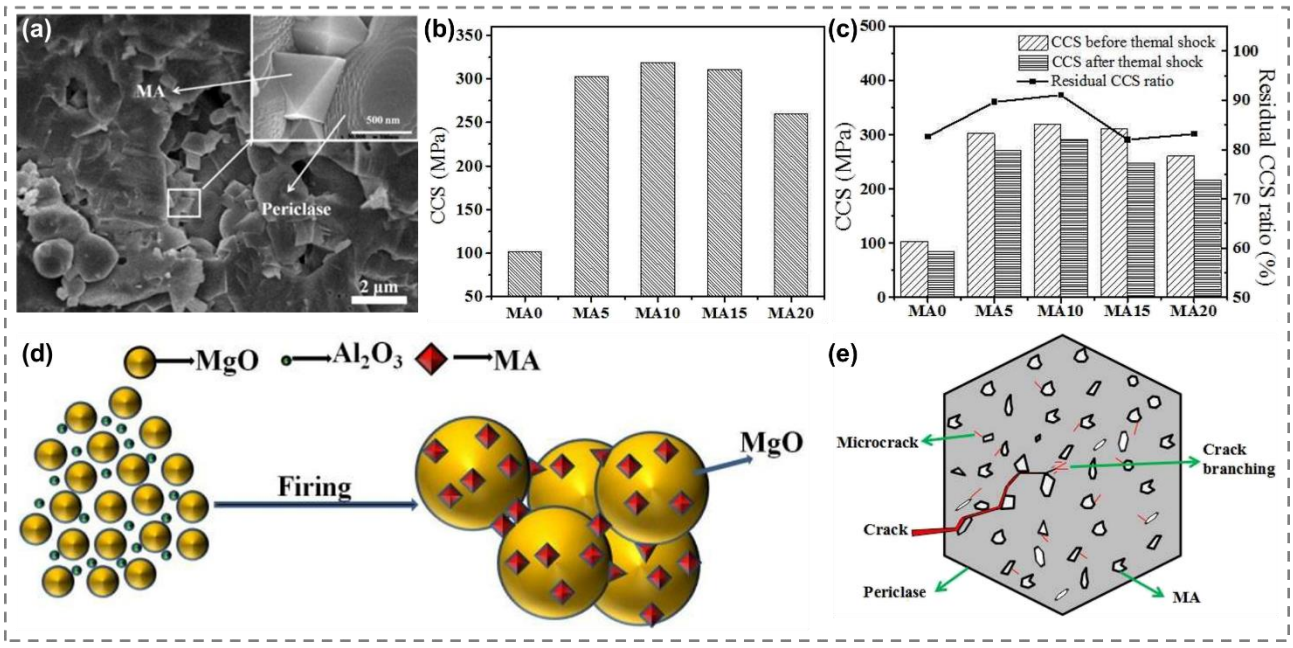

Figure 10. (**a**) SEM microphotographs of samples with 19 wt.% $MgAl_2O$. (**b**) CCS of samples after coked at 1500 °C. (**c**) Residual CCS and residual CCS ratio of samples after coked at 1500 °C. (**d**) Schematic diagram of in situ formation of nano-sized $MgAl_2O_4$ in magnesia aggregates. And (**e**) schematic of crack propagation in samples with the addition of $MgAl_2O_4$ [206]. (**a**–**d**) Copyright 2019, Elsevier.

Nanosized oxides are highly reactive and can promote the formation of new ceramic phases, enhancing the performance of MgO−C refractories. Ghasemi-Kahrizsangi et al. [208] reported that incorporating nano-$ZrSiO_4$ in MgO−C refractories led to the creation of new ceramic phases such as zirconium carbide (ZrC), forsterite ($2MgO{\cdot}SiO_2$), and enstatite ($MgO{\cdot}SiO_2$). The addition of nano-$ZrSiO_4$ increased the bulk density by forming the low-melting phase ($MgO{\cdot}SiO_2$). Additionally, the phases $2MgO{\cdot}SiO_2$ and $MgO{\cdot}SiO_2$ enveloped the free graphite phase, along with the high oxidation resistance phase ZrC, resulting in improved oxidation resistance of MgO−C refractories. The formation of these new ceramic phases filled the pores and voids, preventing slag penetration and enhancing slag corrosion resistance. Furthermore, the impact of adding TiO_2 nanoparticles on the microstructure and properties of MgO−C refractories was investigated [209]. The introduction of TiO_2 nanoparticles resulted in the formation of TiN, TiC, and TiCN phases. These phases enhanced the mechanical, physical, and thermo-chemical properties of the samples through several mechanisms: (i) converting free graphite into carbide and nitride phases, (ii) reducing porosities within the matrix, and (iii) improving the firing process due to the presence of nanoparticles. This enhancement underscores the significant role that nanotechnology plays in advancing refractory materials, especially in settings that require improved durability and resistance to harsh conditions.

Chen et al. [210] demonstrated that the addition of nanosized ZrO_2−Al_2O_3 composite powders can significantly reduce porosity and optimize the pore structure in MgO−C refractories, thanks to their excellent filling capabilities, ultimately enhancing the oxidation resistance and slag corrosion resistance of the refractories. The SEM image depicted in Figure 11a illustrates the sample with 0.5 wt.% ZrO_2−Al_2O_3 composite powders had a well-bonded matrix of plate-like MgO aggregates and uniformly dispersed ZrO_2 particles. MgO−C samples containing these nano ZrO_2−Al_2O_3 composite powders exhibited higher residual strength ratios after thermal shock tests (Figure 11b), demonstrating that the composite powders had a positive impact on thermal shock resistance. The cross-sections and corresponding oxidation indices of different samples after oxidation tests, shown in Figure 11c–f, clearly revealed that with increasing content of nano ZrO_2−Al_2O_3 composite powder, the oxidation indices of the samples gradually decreased. This trend highlights the positive effect of the composite powders on the oxidation resistance of low-carbon MgO−C refractories. Furthermore, after slag corrosion tests, the corrosion indices of the samples, as shown in Figure 11g, indicated that adding composite powders effectively improved the slag corrosion resistance of the low-carbon MgO−C refractories.

This comprehensive enhancement in performance attributes underscores the significant role that nanosized composite powders play in advancing the durability and functionality of refractory materials under severe operating conditions.

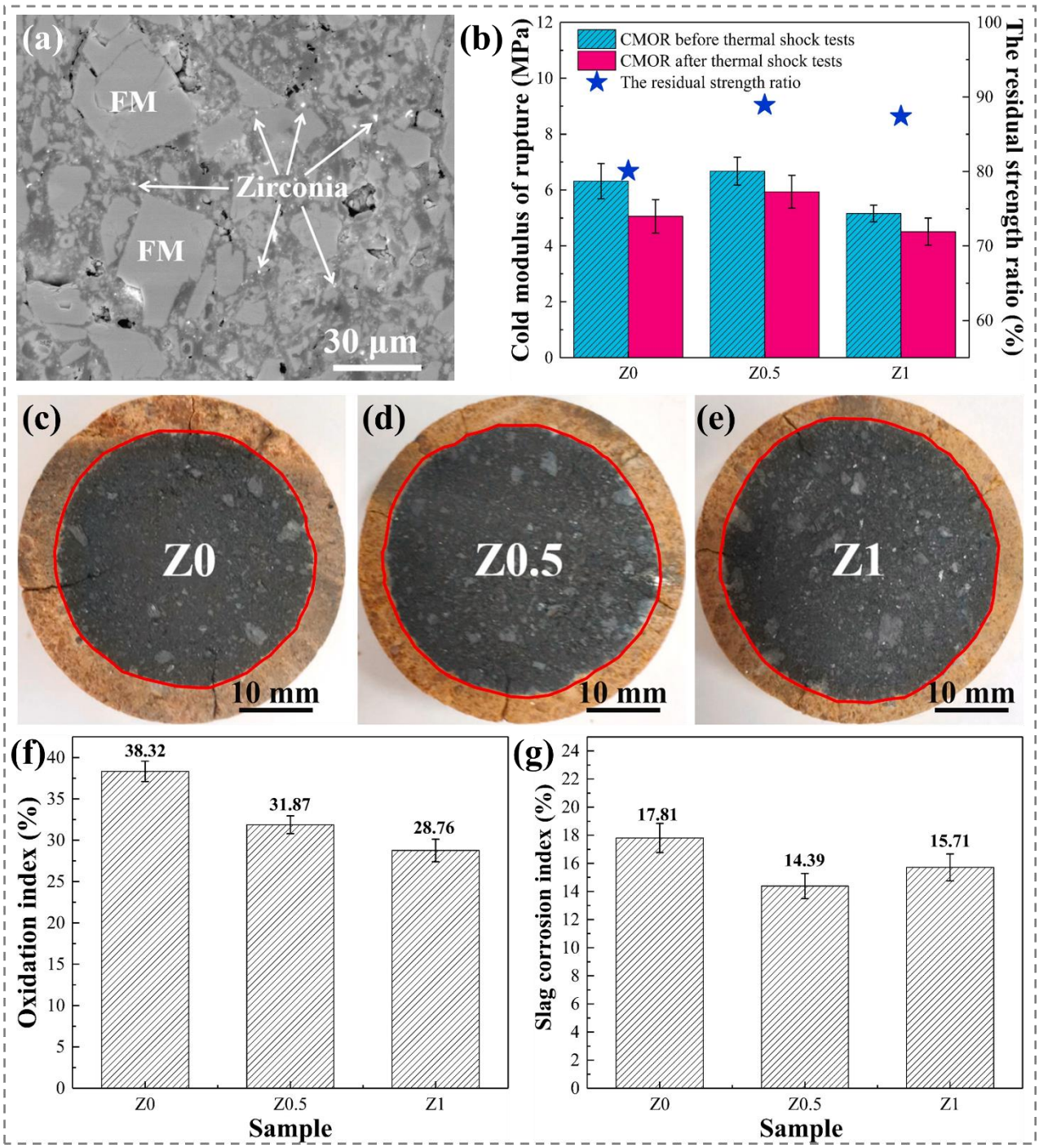

Figure 11. (**a**) SEM micrographs of the polished composite powder with 0.5 wt.% ZrO_2−Al_2O_3 after calcinated at 1400 °C (FM: fused magnesia). (**b**) CMOR and residual strength ratio of specimens after thermal shock tests. (**c**–**e**) Cross-sections of MgO−C specimens fired at 1400 °C for 3 h in air. (**f**) Oxidation index of various specimens after oxidation tests. And (**g**) slag corrosion index of MgO−C specimens after slag corrosion tests [210]. (**a**–**g**) Copyright 2021, Elsevier.

In addition to the aforementioned studies, incorporating nanosized oxides is regarded as a practical and effective approach to enhance the thermal shock resistance and slag corrosion resistance of CCRs. To achieve this, it is essential to choose oxide materials with appropriate phase compositions and thermal expansion coefficients, control the in situ formation of new ceramic phases and thereby improve the overall performance of CCRs.

5. Conclusions

Traditional CCRs possess excellent thermal shock resistance and slag corrosion resistance. However, the high carbon content limits their application due to carbon oxidation and high thermal conductivity. Merely reducing the carbon content results in poor high-temperature service performances. To address this issue, nanomaterial-modified matrix has been developed in CCRs. Due to their unique dimensional structures and physical/chemical properties, nanomaterials as reinforcement additives can significantly improve service performances through deliberate design. Desirable features are achieved owing to the nano-architectonics of nanomaterials in terms of their unique size, shape, and composition. Three classes of nanomaterials are primarily taken into consideration for dispersion in the CCRs matrix: (1) Nanocarbon additives, including carbon black, carbon nanotubes, and graphite nanoplatelets, which are categorized as 0D, 1D and 2D, respectively, depending on their dimensions. (2) Nano oxides, come in powders such as Al_2O_3, MgO, $MgAl_2O_4$ and ZrO_2. And (3) nano non-oxide additives, which are classified as nitride and carbide. Introducing nanocarbon materials into the matrix of refractories can improve the mechanical properties and thermal shock resistance of CCRs. Due to the small particle size and lower density of these nanomaterials, the compactness of refractories is enhanced, and a more effective surface area is achieved. However, nanocarbon materials possess poor oxidation resistance and high reactive activity, which can induce structural alteration. Both direct addition and in situ generation of nano-oxide additives can fill pores and improve the oxidation resistance of refractories, and the newly formed ceramic phases enhance slag resistance. Nano non-oxide additives offer better oxidation and slag corrosion resistance for CCRs, but structural collapse can cause a loss of service performance.

The current status of nanomaterial-reinforced CCRs is reviewed based on available research articles. The future of nanomaterial incorporation in CCRs is very promising. With the continuous improvement in high-performance steel material requirements, recent studies have aimed to understand the behavior of CCRs reinforced with various types of nanomaterials. However, several factors need to be considered in this research field:

1. The reinforcement mechanisms of nanomaterials include energy dissipation mechanisms, “crack deflection,” “pulling out,” and “bridging” mechanisms, which are related to the dimensionality of the nanomaterials. Often, the synergistic effects of multiple mechanisms produce the final results. The precise synergy of different mechanisms and the contribution of any individual mechanism remain unclear. Therefore, designing high-performance nanosized additives should consider nanomaterials physical and chemical properties and their reinforcement mechanisms to optimize service performances.
2. The full potential of nanosized additives, such as carbon nanotubes and graphene nanosheets, is not yet utilized. These additives are consumed and transformed into ceramic phases during the firing process, sacrificing their intrinsic advantages. Functionalizing them and inhibiting the high-temperature reactions are interesting and challenging research areas.
3. Due to the large surface area of nanomaterials, they tend to agglomerate. The literature describes two methods for deagglomeration: in situ synthesis and the addition of nanomaterial-oxide nanocomposite additives. However, these strategies need further investigation and optimization as they are time and resource-consuming, and a new method needs to be developed for this purpose.
4. Despite significant improvement of CCRs properties shown by nanoscale materials addition, the dispersion and retention properties of nanoscale additives and their stability at elevated temperatures and in corrosive environments, require further research. Solving this issue has the potential to significantly improve both the mechanical properties and service life of nanomaterial-reinforced CCRs.
5. The use of nanoscale materials in carbon-bonded refractories is hindered by their extremely high production costs. Nanocomposites incur additional expenses due to their costly production and processing. However, increasing demand and production will help to reduce the cost of nanosized additives.

Although the application of nanoscale additives poses various challenges, ongoing research into improved dispersion techniques, stability-enhancing nanomaterials, reinforcement mechanisms and cost reduction will pave the way for their large-scale application in various fields. Despite these challenges, nanoscale materials show promising prospects for significantly improving the service performances of CCRs.

Author Contributions

Conceptualization, F.L.; Investigation, F.L., H.G. and J.L.; Writing—Original Draft Preparation, F.L.; Writing—Review & Editing, F.L. and J.L.; Supervision, F.L. and H.Z.; Project, F.L. and H.Z.; Funding Acquisition, H.Z.

Ethics Statement

Not applicable.

Informed Consent Statement

Not applicable for studies not involving humans.

Funding

This research was funded by National Natural Science Foundation of China grant number 52072274, 52272021, 52232002 and U23A20559.

Declaration of Competing Interest

The authors declare that they have no known competing financial interests or personal relationships that could have appeared to influence the work reported in this paper.

References

1. Li Y. Effect of alumina-coated graphite (ACG) on the microstructure and mechanical properties of Al_2O_3−C refractories. *J. Ceram. Sci. Technol.* **2017**, *8*, 455–462. doi:10.4416/JCST2016−00079.
2. Xing G, Deng C, Ding J, Ma B, Wang Z, Zhu H, et al. Enhanced mechanical performance of in-situ Mg-sialon in low-carbon MgO−C refractories through Si–Al_4SiC_4 additions. *J. Eur. Ceram. Soc.* **2024**, *44*, 5262–5274. doi:10.1016/j.jeurceramsoc.2024.02.021.
3. Tomeczek J, Suwak R. Thermal conductivity of carbon-containing refractories. *Ceram. Int.* **2002**, 28, 601–607. doi.org/10.1016/S0272−8842(02)00015−9.
4. Wang Q, Li Y, Luo M, Sang S, Zhu T, Zhao L. Strengthening mechanism of graphene oxide nanosheets for Al_2O_3−C refractories. *Ceram. Int.* **2014**, *40*, 163–172. doi:10.1016/j.ceramint.2013.05.117.
5. Xiao G, Yang S, Ding D, Ren Y, Lv L, Yang P, Hou X, Gao J. One-step synthesis of in-situ carbon-containing calcium aluminate cement as binders for refractory castables. *Ceram. Int.* **2018**, *44*, 15378−15384. doi.org/10.1016/j.ceramint.2018.05.189.
6. Wang H, Li Y, Zhu T, Fu Z. Strengthening of Al_2O_3−C slide gate plate refractories with microcrystalline graphite. *Ceram. Int.* **2017**, *43*, 9912–9918. doi:10.1016/j.ceramint.2017.04.178.
7. Stückelschweiger M, Gruber D, Jin S, Harmuth H. Wedge-splitting test on carbon-containing refractories at high temperatures. *Appl. Sci.* **2019**, *9*, 3249. doi.org/10.3390/app9163249.
8. Ding D, Yang S, Xiao G, Ren Y, Lv L, Yang P, et al. Investigations on the properties of A_2O_3−MgO refractory castables bonded by in situ carbon containing calcium aluminate cement. *Mater. Res. Express* **2018**, *5*, 095205. doi:10.1088/2053−1591/aad889.
9. Liu Z, Deng C, Yu C, Wang X, Ding J, Zhu H. Molten salt synthesis and characterization of SiC whiskers containing coating on graphite for application in Al_2O_3−SiC−C castables. *J. Alloys Compd.* **2019**, *777*, 26–33. doi:10.1016/j.jallcom.2018.09.107.
10. Bezerra BP, Luz AP, Pandolfelli VC. Novel drying additives and their evaluation for self-flowing refractory castables. *Ceram. Int.* **2020**, *46*, 3209–3217. doi:10.1016/j.ceramint.2019.10.025.
11. Ding D, Lv L, Xiao G, Luo J, Lei C, Ren Y, et al. Improved properties of low-carbon MgO−C refractories with the addition of multilayer graphene/$MgAl_2$ O_4 composite powders. *Int. J. Appl. Ceram. Technol.* **2020**, *17*, 645–656. doi:10.1111/ijac.13347.
12. Lee J, Myung J, Chung Y. Degradation kinetics of MgO−C refractory at high temperature. *Metall Mater Trans B* **2021**, *52*, 1179–1185. doi.org/10.1007/s11663−021−02106−9.
13. Xu H, Wang X, Zhang W, Deng N. The rapid synthesis of CaB_6 powders by combining induction heating with carbothermic reduction and their antioxidant properties. *J. Aust. Ceram. Soc.* **2021**, *57*, 919–926. doi:10.1007/s41779−021−00586−1.
14. Wang H, Li Y, Zhu T, Sang S, Wang Q. Microstructures and mechanical properties of Al_2O_3−C refractories with addition of microcrystalline graphite. *Ceram. Int.* **2014**, *40*, 11139–11148. doi:10.1016/j.ceramint.2014.03.139.
15. Whittemore OJ, Jr., Marshall DW. Fused stabilized zirconia and refractories. *J. Am. Ceram. Soc.* **1952**, 35, 85–89. doi.org/10.1111/j.1151−2916.1952.tb13076.x.
16. Kumar A, Khanna R, Spink J, Sahajwalla V. Fundamental investigations on the corrosion of ZrO_2−C refractories during interaction with a casting mould meniscus slag. *Steel Res. Int.* **2014**, *85*, 1185–1193. doi:10.1002/srin.201300336.
17. Bie C, Sang S, Li Y, Zhu T, Xu Y. Research of Al_2O_3−SiC−C refractories as chromia-free lining for gasifier. *Ceram. Int.* **2016**, 42, 14161−14167. doi.org/10.1016/j.ceramint.2016.06.038.
18. Yang S, Xiao G, Ding D, Gao J. Effect of in-situ carbon containing calcium aluminate cement on properties of Al_2O_3−SiC−C based trough castables. *J. Asian Ceram. Soc.* **2020**, *8*, 162–169. doi:10.1080/21870764.2020.1718861.

19. Nandy SK, Chaudhuri PKR, Barua P, Halder D, Ghosh NK, Tete B, et al. Customised lining design for improvement in lining life of 150T steel ladle at rourkela steel plant. *Trans. Indian Ceram. Soc.* **2001**, *60*, 172–175. doi:10.1080/0371750X.2001.10799997.
20. Sarkar S, Sahoo MR, Kujur MK, Das UK, Das SK, Reddy TS. Development of metallic fibre-reinforced MgO−C brick and its application at the sail rourkela steel plant. *Interceram—Int. Ceram. Rev.* **2017**, *66*, 38–40. doi:10.1007/BF03401227.
21. Cho G, Byeun Y, Jung Y. Studies on damage properties of MgO−C refractories through hertzian indentation at room and high temperatures. *J. Korean Ceram. Soc.* **2019**, *56*, 77–83. doi:10.4191/kcers.2019.56.1.09.
22. Kundu R, Sarkar R. MgO−C refractories: A detailed review of these irreplaceable refractories in steelmaking. *Interceram−Int. Ceram. Rev.* **2021**, *70*, 46–55. doi:10.1007/s42411−021−0457−9.
23. Atzenhofer C, Gschiel S, Harmuth H. Phase formation in Al_2O_3−C refractories with Al addition. *J. Eur. Ceram. Soc.* **2017**, *37*, 1805–1810. doi:10.1016/j.jeurceramsoc.2016.11.027.
24. Wei X, Yehorov A, Storti E, Dudczig S, Fabrichnaya O, Aneziris CG, et al. Phenomenon of whiskers formation in Al_2O_3−C refractories. *Adv. Eng. Mater.* **2021**, *24*, 2100718. doi:10.1002/adem.202100718.
25. Yu C, Dong B, Deng C, Ding J, Zhu H, Di J. In-situ formation of plate-like Al_4O_4C and MWCNTs in Al_2O_3−C refractories with Al_4SiC_4 additives. *Mater. Chem. Phys.* **2021**, *263*, 124363. doi:10.1016/j.matchemphys.2021.124363.
26. Gao Y, Yu Z, Guo C, Wang E, Liu X, Xu E, et al. Improving the comprehensive properties of ZrO_2−C materials with aid of TiO_2 addition. *Ceram. Int.* **2024**, *50*, 17720–17726. doi:10.1016/j.ceramint.2024.02.260.
27. Gu Q, Wang Q, Ma F, Liu G, Yuan L, Li H. Effect of applied electric field on corrosion resistance of slag-line (ZrO_2−C material) of SEN under near working condition. *J. Eur. Ceram. Soc.* **2024**, *44*, 1814–1824. doi:10.1016/j.jeurceramsoc.2023.10.005.
28. Yang X, He Z, Yu J, Zhang Y, Yuan L, Mao F. Influence of interface electric field on interaction between molten iron and refractory interface. *Ceram. Int.* **2020**, *46*, 10180–10185. doi:10.1016/j.ceramint.2020.01.009.
29. Wu M, Huang A, Yang S, Gu H, Fu L, Li G, et al. Corrosion mechanism of Al_2O_3−SiC−C refractory by SiO_2−MgO−based slag. *Ceram. Int.* **2020**, *46*, 28262–28267. doi:10.1016/j.ceramint.2020.07.327.
30. Chen A, Fu Y, Mu Y, Wang Q, Parr C, Ye G. Oxidation resistance of andalusite-bearing Al_2O_3−SiC−C castables containing reduced anti-oxidant. *Ceram. Int.* **2021**, *47*, 14579–14586. doi:10.1016/j.ceramint.2021.02.039.
31. Ding D, Tian X, Ye G, Touzo B, Ahouanto F, Parr C. Effect of andalusite aggregates on oxidation resistance of Al_2O_3−SiC−C castables. *Ceram. Int.* **2019**, *45*, 19237–19241. doi:10.1016/j.ceramint.2019.06.171.
32. Luz AP, Renda CG, Lucas AA, Bertholdo R, Aneziris CG, Pandolfelli VC. Graphitization of phenolic resins for carbon-based refractories. *Ceram. Int.* **2017**, *43*, 8171–8182. doi:10.1016/j.ceramint.2017.03.143.
33. Nanda S, Choudhury A, Chandra KS, Sarkar D. Raw materials, microstructure, and properties of MgO−C refractories: Directions for refractory recipe development. *J. Eur. Ceram. Soc.* **2023**, *43*, 14–36. doi:10.1016/j.jeurceramsoc.2022.09.032.
34. Hussain MA, Faisal M, Raza K, Rafiq MA, Usman M, Amin W, et al. Development and characterization of nano-magnesia-based refractories filled with graphite nanosheets. *Ceram. Int.* **2024**, *50*, 12724–12731. doi:10.1016/j.ceramint.2024.01.176.
35. Chandra KS, Sarkar D. Strong and tough Al_2O_3−MgO−C refractories with dispersed aluminosilicate reinforcement. *Mater. Chem. Phys.* **2022**, *277*, 125493. doi:10.1016/j.matchemphys.2021.125493.
36. Mukhopadhyay S, Dutta S, Ansar SA, Das S, Misra S. Spinel-coated graphite for carbon containing refractory castables. *J. Am. Ceram. Soc.* **2009**, *92*, 1895–1900. doi:10.1111/j.1551−2916.2009.03133.x.
37. Bi Y, Zhang H, Wang H, Duan S, Jia Q, Ge S, et al. Catalytic Fabrication of SiC/SiO_2 coated graphite and its behavior in Al_2O_3−C castable systems. *Ceram. Int.* **2019**, *45*, 16180–16187. doi:10.1016/j.ceramint.2019.05.139.
38. Li S, Liu J, Wang J, Han L, Zhang H, Zhang S. Catalytic preparation of graphitic carbon spheres for Al_2O_3−SiC−C castables. *Ceram. Int.* **2018**, *44*, 12940–12947. doi:10.1016/j.ceramint.2018.04.108.
39. Zhang S, Lee WE. Carbon containing castables: Current status and future prospects. *Br. Ceram. Trans.* **2002**, *101*, 1–8. doi:10.1179/096797801125000410.
40. Zhang Y, Bu A, Xiang Y, Yang Y, Chen W, Cheng H, et al. Cubic γ-Al_2O_3 coating modified graphite powder. *Vacuum* **2020**, *181*, 109739. doi:10.1016/j.vacuum.2020.109739.
41. Aneziris CG, Borzov D, Ulbricht J. Magnesia−carbon bricks: A high duty refractory material. *Interceram. Refract. Manual* **2003**, *52*, 22–27.
42. Tamura S, Ochiai T, Takanaga S, Kanai T, Nakamura H. Nano-tech refractories-1: The development of the nano structural matrix. In Proceedings of theUNITECR'2003 Congress, Osaka, Japan, 19–22 October 2003; pp. 517–520.
43. Behera S, Sarkar R. Nano carbon containing low carbon magnesia carbon refractory: An overview. *Prot. Met. Phys. Chem. Surf.* **2016**, *52*, 467–474. doi:10.1134/S2070205116030059.
44. Bag M, Adak S, Sarkar R. Study on low carbon containing MgO−C refractory: Use of nano carbon. *Ceram. Int.* **2012**, *38*, 2339–2346. doi:10.1016/j.ceramint.2011.10.086.
45. Pilli V, Sarkar R. Effect of mixing on the properties of nanocarbon containing Al_2O_3−C continuous casting refractories. *Int. J. Appl. Ceram. Technol.* **2020**, *17*, 637–644. doi:10.1111/ijac.13331.

46. Bahtli T, Hopa DY, Bostanci VM, YalcinYasti S. Thermal conductivity of MgO−C refractory ceramics: Effects of pyrolytic liquid and pyrolytic carbon black obtained from waste tire. *Ceram. Int.* **2018**, *44*, 13848–13851. doi:10.1016/j.ceramint.2018.04.230.
47. Wang Y, Wu Y, Peng B, Wu K, Zhang G. A universal method for the synthesis of refractory metal diborides. *Ceram. Int.* **2021**, *47*, 14107–14114. doi:10.1016/j.ceramint.2021.01.281.
48. Wan Q, Yin H, Tang Y, Yuan H, Ren X, Xin Y, et al. Effect of carbon sources on the properties of lightweight corundum-spinel refractory with density gradient. *Int. J. Appl. Ceram. Technol.* **2020**, *17*, 598–605. doi:10.1111/ijac.13437.
49. Chen J, Li N, Wei Y, Han B, Yan W. Influence of carbon sources on nitriding process, microstructures and mechanical properties of Si_3N_4 bonded SiC refractories. *J. Eur. Ceram. Soc.* **2017**, *37*, 1821–1829. doi:10.1016/j.jeurceramsoc.2016.12.005.
50. Mao J, Sun L, Lv J, Tan Y. Piezoelectric and dielectric behavior of 0−3 asphalt-based composites with carbon black. *Ceram. Int.* **2016**, *42*, 16132–16137. doi:10.1016/j.ceramint.2016.07.130.
51. Chollakup R, Suethao S, Suwanruji P, Boonyarit J, Smitthipong W. Mechanical properties and dissipation energy of carbon black/rubber composites. *Compos. Adv. Mater.* **2021**, *30*, 1–6. doi:10.1177/26349833211005476.
52. Cha JH, Shin G−J, Kang M−J, Lee HI, Rhee KY, Park S−J. A study on the effect of electron acceptor-donor interactions on the mechanical and interfacial properties of carbon black/natural rubber composites. *Compos. Part B Eng.* **2018**, *136*, 143–148. doi:10.1016/j.compositesb.2017.10.003.
53. Chauhan S, Bhushan RK. Improvement in mechanical performance due to hybridization of carbon fiber/epoxy composite with carbon black. *Adv. Compos. Hybrid Mater.* **2018**, *1*, 602–611. doi:10.1007/s42114−018−0047−0.
54. Afzal A, Kausar A, Siddiq M. Perspectives of polystyrene composite with fullerene, carbon black, graphene, and carbon nanotube: A review. *Polym. −Plast. Technol. Eng.* **2016**, *55*, 1988–2011. doi:10.1080/03602559.2016.1185632.
55. Pilli V, Priyadarshini S, Sarkar R. Nanocarbon containing low carbon Al_2O_3−C refractories: Comparison between N220 and N990 nanocarbons. *Int. J. Appl. Ceram. Technol.* **2022**, *19*, 2761–2779. doi:10.1111/ijac.14120.
56. Wu M, Huang A, Chen D, Fu L, Gu H. Effect of carbon black on corrosion resistance of Al_2O_3−SiC−C castables to SiO_2−MgO slag. *Ceram. Int.* **2022**, *48*, 13659–13664. doi:10.1016/j.ceramint.2022.01.245.
57. Li YW. Microstructure and mechanical properties of Al_2O_3−C refractories using carbon black and multi-walled carbon nanotubes as carbon sources. *J. Ceram. Sci. Tech.* **2015**, *6*, 207–214. doi:10.4416/JCST2015−00003.
58. Liao N, Li Y, Jin S, Sang S, Harmuth H. Enhanced mechanical performance of Al_2O_3−C refractories with nano carbon black and in-situ formed multi-walled carbon nanotubes (MWCNTs). *J. Eur. Ceram. Soc.* **2016**, *36*, 867–874. doi:10.1016/j.jeurceramsoc.2015.10.003.
59. Bag M, Adak S, Sarkar R. Nano carbon containing MgO−C refractory: Effect of graphite content. *Ceram. Int.* **2012**, *38*, 4909–4914. doi:10.1016/j.ceramint.2012.02.082.
60. Maio A, Pibiri I, Morreale M, Mantia F, Scaffaro R. An overview of functionalized graphene nanomaterials for advanced applications. *Nanomaterials* **2021**, *11*, 1717. doi:10.3390/nano11071717.
61. Ye J, Zhang S, Lee WE. Molten salt synthesis and characterization of SiC coated carbon black particles for refractory castable applications. *J. Eur. Ceram. Soc.* **2013**, *33*, 2023–2029. doi:10.1016/j.jeurceramsoc.2013.02.011.
62. Najafi A. Facile and scalable synthesis of uniform MgO/Carbon Black nano-admixture for microstructural and mechanical property improvement of magnesia−carbon refractory bricks. *Ceram. Int.* **2016**, *42*, 18031–18036. doi:10.1016/j.ceramint.2016.08.065.
63. Yang Y, Yu J, Zhao H, Zhang H, Zhao P, Li Y, et al. Cr_7C_3: A potential antioxidant for low carbon MgO−C refractories. *Ceram. Int.* **2020**, *46*, 19743–19751. doi:10.1016/j.ceramint.2020.04.298.
64. Zhao SM, Mei GH, Zhang J. Effects of antioxidants particle size on oxidation resistance of MgO−C refractory. *Key Eng. Mater.* **2019**, *821*, 452–456. doi:10.4028/www.scientific.net/KEM.821.452.
65. Wang X, Deng C, Di J, Xing G, Ding J, Zhu H, et al. Enhanced oxidation resistance of low-carbon MgO−C refractories with Al_3BC_3−Al antioxidants: A synergistic effect. *J. Am. Ceram. Soc.* **2023**, *106*, 3749–3764. doi:10.1111/jace.19023.
66. Luz AP, Souza TM, Pagliosa C, Brito MAM, Pandolfelli VC. In-situ hot elastic modulus evolution of MgO−C refractories containing Al, Si or Al−Mg antioxidants. *Ceram. Int.* **2016**, *42*, 9836–9843. doi:10.1016/j.ceramint.2016.03.080.
67. Xiao J, Chen J, Wei Y, Zhang Y, Zhang S, Li N. Oxidation behaviors of MgO−C refractories with different Si/SiC ratio in the 1100–1500 °C range. *Ceram. Int.* **2019**, *45*, 21099–21107. doi:10.1016/j.ceramint.2019.07.086.
68. Atzenhofer C, Harmuth H. Phase formation in MgO−C refractories with different antioxidants. *J. Eur. Ceram. Soc.* **2021**, *41*, 7330–7338. doi:10.1016/j.jeurceramsoc.2021.07.023.
69. Zhang Y, Chen J, Li N, Wei Y, Han B, Cao Y, et al. The microstructure evolution and mechanical properties of MgO−C refractories with recycling Si/SiC solid waste from photovoltaic industry. *Ceram. Int.* **2018**, *44*, 16435–16442. doi:10.1016/j.ceramint.2018.06.057.
70. Behera S, Sarkar R. Effect of different metal powder anti-oxidants on N220 nano carbon containing low carbon MgO−C refractory: An in-depth investigation. *Ceram. Int.* **2016**, *42*, 18484–18494. doi:10.1016/j.ceramint.2016.08.185.

71. Luo J, Jin S, Chong X, Ding D, Xiao G. Brittleness reduction of low-carbon Al_2O_3−C refractories with in-situ formation $MgAl_2O_4$/CNTs layer between aggregate and matrix. *J. Eur. Ceram. Soc.* **2024**, *44*, 2620–2629. doi:10.1016/j.jeurceramsoc.2023.11.060.
72. Chen Z, Yan W, Schafföner S, Li Y, Nath M, Zhu C. Enhanced mechanical properties of lightweight Al_2O_3−C refractories reinforced by combined one-dimensional ceramic phases. *Int. J. Appl. Ceram. Technol.* **2022**, *19*, 1613–1625. doi:10.1111/ijac.13933.
73. Negri V, Pacheco−Torres J, Calle D, López−Larrubia P. Carbon nanotubes in biomedicine. *Top Curr Chem.* **2020**, *378*, 15. doi.org/10.1007/s41061−019−0278−8.
74. Ding D, Zhao Y, Dong S, Yu P, Wang L, Zhao J. The vibration of a linear carbon chain in carbon nanotubes. *Materials* **2017**, *10*, 478. doi:10.3390/ma10050478.
75. Popov VN. Carbon nanotubes: Properties and application. *Mat. Sci. Eng. R* **2004**, *43*, 61–102. doi:10.1016/j.mser.2003.10.001.
76. Wang Y, Zhang W, Zeng X, Huang J, Chen Y, Wei H, et al. Study on microstructures and mechanical strength of MgO−C refractories with cobalt-loaded expanded graphite. *Int. J. Appl. Ceram. Technol*. **2023**, *21*, 2312–2320. doi:10.1111/ijac.14622.
77. Simoes FRF, Abou−Hamad E, Kamenik J, Kučera J, Costa PMFJ. The elemental analysis and multi-nuclear NMR study of an alkali molten salt used to digest reference and commercial SWCNT powders. *J. Anal. At. Spectrom.* **2020**, *35*, 2758–2769. doi:10.1039/D0JA00325E.
78. Halder D, Midya PR, Das S, Das NS, Roy I, Chattopadhyay KK. Amorphous carbon nanotubes incorporated MgO−graphite composite with enhanced properties for steel making furnaces. *Ceram. Int.* **2016**, *42*, 15826–15835. doi:10.1016/j.ceramint.2016.07.051.
79. Luo M, Li Y, Jin S, Sang S, Zhao L, Li Y. Microstructures and mechanical properties of Al_2O_3−C refractories with addition of multi-walled carbon nanotubes. *Mater. Sci. Eng. A* **2012**, *548*, 134–141. doi:10.1016/j.msea.2012.04.001.
80. Luo M, Li Y, Jin S, Sang S, Zhao L, Wang Q, et al. Microstructure and mechanical properties of multi-walled carbon nanotubes containing Al_2O_3−C refractories with addition of polycarbosilane. *Ceram. Int.* **2013**, *39*, 4831–4838. doi:10.1016/j.ceramint.2012.11.075.
81. Liao N, Li Y, Jin S, Xu Y, Sang S, Deng Z. Combined effects of boron carbide, silicon, and MWCNTs in alumina−carbon refractories on their microstructural evolution. *J. Am. Ceram. Soc.* **2017**, *100*, 443–450. doi:10.1111/jace.14543.
82. Luo W, Zhu B, Li X, Chen P, Ma Z, Wang X. In-situ formation of MgO whiskers and CNTs and their influence on the mechanical properties of low-carbon MgO−C refractory composites. *Int. J. Mater. Res.* **2016**, *107*, 333–339. doi:10.3139/146.111344.
83. Liao N, Li Y, Jin S, Sang S, Liu G. Reduced brittleness of multi-walled carbon nanotubes (MWCNTs) containing Al_2O_3−C refractories with boron carbide. *Mater. Sci. Eng. A* **2017**, *698*, 80–87. doi:10.1016/j.msea.2017.05.045.
84. Wei G, Zhu B, Li X, Ma Z. Microstructure and mechanical properties of low-carbon MgO−C refractories bonded by an Fe nanosheet-modified phenol resin. *Ceram. Int.* **2015**, *41*, 1553–1566. doi:10.1016/j.ceramint.2014.09.091.
85. Zhu T, Li Y, Sang S, Xie Z. Formation of nanocarbon structures in MgO−C refractories matrix: Influence of Al and Si additives. *Ceram. Int.* **2016**, *42*, 18833–188843. doi:10.1016/j.ceramint.2016.09.029.
86. Feng C, Xiao G, Ding D, Lei C, Lv L, Chong X, et al. Enhanced thermal shock resistance of low-carbon A_2O_3−C refractories via CNTs/$MgAl_2O_4$ whiskers composite reinforcement. *J. Am. Ceram. Soc.* **2024**, *107*, 3881–3894. doi:10.1111/jace.19673.
87. Li G, Ding D, Xiao G, Jin E, Luo J, Lei C. Catalytic combustion synthesis of CNTs/MgO composite powders and the influences on the thermal shock resistance of low-carbon Al_2O_3−C refractories. *Ceram. Int.* **2022**, *48*, 10601–10612. doi:10.1016/j.ceramint.2021.12.274.
88. Liang F, Li N, Liu B, He Z. Processing and characterization of multi-walled carbon nanotubes con88taining alumina−carbon refractories prepared by nanocomposite powder technology. *Metall. Mater. Trans. B* **2016**, *47*, 1661–1668. doi:10.1007/s11663−016−0647−4.
89. Li Y, Shan J, Liao N, Sang S, Jia D. Enhanced thermal shock resistance of low-carbon Al_2O_3−C refractories with direct CVD synthesis of nano carbon decorated oxides. *J. Eur. Ceram. Soc.* **2018**, *38*, 3379–3386. doi:10.1016/j.jeurceramsoc.2018.02.042.
90. Yang L, Wang D, Liu M, Liu H, Tan J, Wang Z, et al. Glue-assisted grinding exfoliation of large-size 2D materials for insulating thermal conduction and large-current-density hydrogen evolution. *Mater. Today* **2021**, *51*, 145–154. doi:10.1016/j.mattod.2021.08.009.
91. Abhervé A, Mañas−Valero S, Clemente−León M, Coronado E. Graphene related magnetic materials: Micromechanical exfoliation of 2D layered magnets based on bimetallic anilate complexes with inserted $[Fe^{III}(acac_2-trien)]^+$ and $[Fe^{III}(sal_2-trien)]^+$ molecules. *Chem. Sci.* **2015**, *6*, 4665–4673. doi:10.1039/C5SC00957J.
92. Costa MCFD, Ribeiro HB, Kessler F, Souza EATD, Fechine GJM. Micromechanical exfoliation of two-dimensional materials by a polymeric stamp. *Mater. Res. Express* **2016**, *3*, 025303. doi:10.1088/2053−1591/3/2/025303.
93. Singh R, Tripathi CC. A comparative study of organic solvents, ionic liquids, surfactants and acids for liquid phase exfoliation of graphene. *Ion. Liq.* **2019**, *57*, 322–333.
94. Ding J, Zhao H, Yu H. A water-based green approach to large−scale production of aqueous compatible graphene nanoplatelets. *Sci. Rep.* **2018**, *8*, 5567. doi:10.1038/s41598−018−23859−5.

95. Nacken TJ, Damm C, Walter J, Rüger A, Peukert W. Delamination of graphite in a high pressure homogenizer. *RSC Adv.* **2015**, *5*, 57328–57338. doi:10.1039/C5RA08643D.
96. Khanam Z, Liu J, Song S. High-concentration graphene dispersions prepared via exfoliation of graphite in PVA/H_2O green solvent system using high-shear forces. *J. Nanopart. Res.* **2021**, *23*, 170. doi:10.1007/s11051−021−05294−2.
97. Liang B, Liu K, Liu P, Zhao G, Pan W, Hu S. Improved efficiency of liquid-phase shear exfoliation of expanded graphite with mica plates as bifunctional additives. *J. Mater. Chem. A* **2021**, *9*, 27586–27595. doi:10.1039/D1TA07915H.
98. Norimatsu W, Kusunoki M. Epitaxial graphene on SiC{0001}: Advances and perspectives. *Phys. Chem. Chem. Phys.* **2014**, *16*, 3501. doi:10.1039/c3cp54523g.
99. Lin Y−M, Dimitrakopoulos C, Jenkins KA, Farmer DB, Chiu H−Y, Grill A, et al. 100−GHz transistors from wafer−scale epitaxial graphene. *Science* **2010**, *327*, 662–662. doi:10.1126/science.1184289.
100. Wazir AH, Kundi IW, Khan WN, Manan A, Querashi I, Yaqoob K. Synthesis and characterization of graphene sheets from graphite through electrochemical exfoliation and microwave reduction. *Key Eng. Mater.* **2021**, *875*, 127–137. doi:10.4028/www.scientific.net/KEM.875.127.
101. Dalal MH, Lee C, Wallace GG. Simultaneous anodic and cathodic exfoliation of graphite electrodes in an aqueous solution of inorganic salt. *ChemElectroChem* **2021**, *8*, 3168–3173. doi:10.1002/celc.202100495.
102. Tkachev S, Monteiro M, Santos J, Placidi E, Hassine MB, Marques P, et al. Environmentally friendly graphene inks for touch screen sensors. *Adv. Funct. Mater.* **2021**, *31*, 2103287. doi:10.1002/adfm.202103287.
103. Ismail Z, Idris WFW, Abdullah AH. From shear exfoliation of graphite in Coca-Cola® to few-layer graphene for smart ink. *Ceram. Int.* **2021**, *47*, 23309–23317. doi:10.1016/j.ceramint.2021.05.044.
104. Amri A, Hendri YB, Yin C, Rahman M, Altarawneh M, Jiang Z. Very-few-layer graphene obtained from facile two-step shear exfoliation in aqueous solution. *Chem. Eng. Sci.* **2021**, *245*, 116848. doi:10.1016/j.ces.2021.116848.
105. Lee T−R. Quantitative correlation between interlayer distance and shear rate in liquid-based exfoliation of graphene layers. *Carbon* **2018**, *129*, 661–666. doi:10.1016/j.carbon.2017.12.068.
106. Piras CC, Fernández−Prieto S, De Borggraeve WM. Ball milling: A green technology for the preparation and functionalisation of nanocellulose derivatives. *Nanoscale Adv.* **2019**, *1*, 937–947. doi:10.1039/C8NA00238J.
107. Mahmoud AED, Stolle A, Stelter M. Sustainable synthesis of high-surface-area graphite oxide via dry ball milling. *ACS Sustain. Chem. Eng.* **2018**, *6*, 6358–6369. doi:10.1021/acssuschemeng.8b00147.
108. Dash P, Dash T, Rout TK, Sahu AK, Biswal SK, Mishra BK. Preparation of graphene oxide by dry planetary ball milling process from natural graphite. *RSC Adv.* **2016**, *6*, 12657–12668. doi:10.1039/C5RA26491J.
109. Zhao W, Fang M, Wu F, Wu H, Wang L, Chen G. Preparation of graphene by exfoliation of graphite using wet ball milling. *J. Mater. Chem.* **2010**, *20*, 5817. doi:10.1039/c0jm01354d.
110. Rico J, Castaño−Soto M, Lopez−Arango N, Hernandez Y. Influence of C=O groups on the optical extinction coefficient of graphene exfoliated in liquid phase. *J. Phys. Condens. Matter* **2022**, *34*, 105701. doi:10.1088/1361−648X/ac3fd6.
111. Gomez CV, Guevara M, Tene T, Villamagua L, Usca GT, Maldonado F, et al. The liquid exfoliation of graphene in polar solvents. *Appl. Surf. Sci.* **2021**, *546*, 149046. doi:10.1016/j.apsusc.2021.149046.
112. Yu P, Wang X, Zhang K, Zhou D, Wu M, Wu Q, et al. Aqueous cellulose solution assisted direct exfoliation of graphite to high concentration graphene dispersion. *Mater. Lett.* **2021**, *285*, 129081. doi:10.1016/j.matlet.2020.129081.
113. Liu K, Hu J, Kong Z, Hu J, Tian Z, Hou J, et al. High-yield, high-conductive graphene/nanocellulose hybrids prepared by co-exfoliation of low-oxidized expanded graphite and microfibrillated cellulose. *Compos. Part B Eng.* **2021**, *225*, 109250. doi:10.1016/j.compositesb.2021.109250.
114. Wu Y, Liu X, Xia D, Sun Q, Yu D, Sun S, et al. Synthesis of few-layer N-doped graphene from expandable graphite with melamine and its application in supercapacitors. *Chin. Chem. Lett.* **2020**, *31*, 559–564. doi:10.1016/j.cclet.2019.04.055.
115. Chernysheva MN, Rychagov AY, Kornilov DY, Tkachev SV, Gubin SP. Investigation of sulfuric acid intercalation into thermally expanded graphite in order to optimize the synthesis of electrochemical graphene oxide. *J. Electroanal. Chem.* **2020**, *858*, 113774. doi:10.1016/j.jelechem.2019.113774.
116. Mahato S, Pratihar SK, Behera SK. Fabrication and properties of MgO−C refractories improved with expanded graphite. *Ceram. Int.* **2014**, *40*, 16535–16542. doi:10.1016/j.ceramint.2014.08.007.
117. Behera SK, Mishra B. Strengthening of Al_2O_3−C slide gate plate refractories with expanded graphite. *Ceram. Int.* **2015**, *41*, 4254–4259. doi:10.1016/j.ceramint.2014.11.092.
118. Kim J, Jeong S, Lee M, Kang DJ, Park H, Lee H, et al. Effects of expanded graphite content on the performance of MgO−C refractories. *Int. J. Appl. Ceram. Technol.* **2023**, *20*, 3803–3813. doi:10.1111/ijac.14464.
119. Wang Q, Li Y, Jin S, Sang S, Xu Y, Xu X, et al. Enhanced mechanical properties of Al_2O_3−C refractories with silicon hybridized expanded graphite. *Mater. Sci. Eng. A* **2018**, *709*, 160–171. doi:10.1016/j.msea.2017.10.046.
120. Lin T, Huang F, Liang J, Wang Y. A facile preparation route for boron-doped graphene, and its CdTe solar cell application. *Energy Env. Sci* **2011**, *4*, 862–865. doi:10.1039/C0EE00512F.
121. Bai J, Zhu Q, Lv Z, Dong H, Yu J, Dong L. Nitrogen-doped graphene as catalysts and catalyst supports for oxygen reduction in both acidic and alkaline solutions. *Int. J. Hydrogen Energy* **2013**, *38*, 1413–1418. doi:10.1016/j.ijhydene.2012.11.039.

122. Sheng Z, Gao H, Bao W, Wang F, Xia X. Synthesis of boron doped graphene for oxygen reduction reaction in fuel cells. *J. Mater. Chem.* **2012**, *22*, 390–395. doi:10.1039/C1JM14694G.
123. Teng C, Xie D, Wang J, Yang Z, Ren G, Zhu Y. Ultrahigh conductive graphene paper based on ball-milling exfoliated graphene. *Adv. Funct. Mater.* **2017**, *27*, 1700240. doi:10.1002/adfm.201700240.
124. Asli AEN, Guo J, Lai PL, Montazami R, Hashemi NN. High-yield production of aqueous graphene for electrohydrodynamic drop-on-demand printing of biocompatible conductive patterns. *Biosensors* **2020**, *10*, 6. doi:10.3390/bios10010006.
125. Wang S, Liang Z, Liu L, Cao Y, Cheng Y, Chen D. Preparation of chemically functionalized graphene with excellent dispersibility and tribological properties as lubricant additives by microwave-assisted ball milling. *J. Mol. Liq.* **2021**, *344*, 117929. doi:10.1016/j.molliq.2021.117929.
126. Wang Q, Li Y, Liao N, Xu X, Sang S, Xu Y, et al. Synthesis of boron and nitrogen-doped expanded graphite as efficient reinforcement for Al_2O_3−C refractories. *Ceram. Int.* **2017**, *43*, 16710–16721. doi:10.1016/j.ceramint.2017.09.063.
127. Chang C, Chen W, Chen Y, Chen Y, Chen Y, Ding F, et al. Recent progress on two-dimensional materials. *Acta Phys. Chim. Sin.* **2021**, *37*, 2108017. doi:10.3866/PKU.WHXB202108017.
128. Sumdani MG, Islam MR, Yahaya ANA, Safie SI. Recent advances of the graphite exfoliation processes and structural modification of graphene: A review. *J. Nanopart. Res.* **2021**, *23*, 253. doi:10.1007/s11051−021−05371−6.
129. Backes C, Abdelkader AM, Alonso C, Andrieux−Ledier A, Arenal R, Azpeitia J, et al. Production and processing of graphene and related materials. *2D Mater.* **2020**, *7*, 022001. doi:10.1088/2053−1583/ab1e0a.
130. Ma H, Shen Z. Exfoliation of graphene nanosheets in aqueous media. *Ceram. Int.* **2020**, *46*, 21873–21887. doi:10.1016/j.ceramint.2020.05.314.
131. Yi M, Shen Z. A review on mechanical exfoliation for the scalable production of graphene. *J. Mater. Chem. A* **2015**, *3*, 11700–11715. doi:10.1039/C5TA00252D.
132. Allen MJ, Tung VC, Kaner RB. Honeycomb carbon: A review of graphene. *Chem. Rev.* **2010**, *110*, 132–145. doi:10.1021/cr900070d.
133. Novoselov KS, Fal VI, Colombo L, Gellert PR, Schwab MG, Kim K. A roadmap for graphene. *Nature* **2012**, *490*, 192–200. doi:10.1038/nature11458.
134. Lin L, Peng H, Liu Z. Synthesis challenges for graphene industry. *Nat. Mater.* **2019**, *18*, 520–524. doi:10.1038/s41563−019−0341−4.
135. Parviz D, Irin F, Shah SA, Das S, Sweeney CB, Green MJ. Challenges in liquid-phase exfoliation, processing, and assembly of pristine graphene. *Adv. Mater.* **2016**, *28*, 8796–8818. doi:10.1002/adma.201601889.
136. Su C, Lu A, Xu Y, Chen F, Khlobystov AN, Li L. High−quality thin graphene films from fast electrochemical exfoliation. *ACS Nano* **2011**, *5*, 2332–2339. doi:10.1021/nn200025p.
137. Alinejad B, Mahmoodi K. Synthesis of graphene nanoflakes by grinding natural graphite together with NaCl in a planetary ball mill. *Funct. Mater. Lett.* **2017**, *10*, 1750047. doi:10.1142/S1793604717500473.
138. Liang B, Liu K, Liu P, Qian L, Zhao G, Pan W, et al. Organic salt-assisted liquid-phase shear exfoliation of expanded graphite into graphene nanosheets. *J. Mater.* **2021**, *7*, 1181–1189. doi:10.1016/j.jmat.2021.03.007.
139. Zhou M, Tang J, Cheng Q, Xu G, Cui P, Qin L−C. Few-layer graphene obtained by electrochemical exfoliation of graphite cathode. *Chem. Phys. Lett.* **2013**, *572*, 61–65. doi:10.1016/j.cplett.2013.04.013.
140. Mao X, Zhu L, Liu H, Chen H, Ju P, Li W. Synthesis of graphene via electrochemical exfoliation in different electrolytes for direct electrodeposition of a Cu/graphene composite coating. *RSC Adv.* **2019**, *9*, 35524–35531. doi:10.1039/C9RA06541E.
141. Yang Q, Zhou M, Yang M, Zhang Z, Yu J, Zhang Y, et al. High-yield production of few-layer graphene via new-fashioned strategy combining resonance ball milling and hydrothermal exfoliation. *Nanomaterials* **2020**, *10*, 667. doi:10.3390/nano10040667.
142. Hass J, Feng R, Li T, Li X, Zong Z, De Heer WA, et al. Highly ordered graphene for two dimensional electronics. *Appl. Phys. Lett.* **2006**, *89*, 143106. doi:10.1063/1.2358299.
143. Tyurnina AV, Tzanakis I, Morton J, Mi J, Porfyrakis K, Maciejewska BM, et al. Ultrasonic exfoliation of graphene in water: A key parameter study. *Carbon* **2020**, *168*, 737–747. doi:10.1016/j.carbon.2020.06.029.
144. Liu Y, Li R. Study on ultrasound-assisted liquid-phase exfoliation for preparing graphene-like molybdenum disulfide nanosheets. *Ultrason. Sonochem.* **2020**, *63*, 104923. doi:10.1016/j.ultsonch.2019.104923.
145. Biccai S, Barwich S, Boland D, Harvey A, Hanlon D, McEvoy N, et al. Exfoliation of 2D materials by high shear mixing. *2D Mater.* **2018**, *6*, 015008. doi:10.1088/2053−1583/aae7e3.
146. Yi M, Shen Z. Kitchen blender for producing high-quality few-layer graphene. *Carbon* **2014**, *78*, 622–626. doi:10.1016/j.carbon.2014.07.035.
147. Zhu T, Li Y, Luo M, Sang S, Wang Q, Zhao L, et al. Microstructure and mechanical properties of MgO−C refractories containing graphite oxide nanosheets (GONs). *Ceram. Int.* **2013**, *39*, 3017–3025 doi:10.1016/j.ceramint.2012.09.080.
148. Lv L, Xiao G, Ding D. Improved thermal shock resistance of low-carbon Al_2O_3−C refractories fabricated with C/$MgAl_2O_4$ composite powders. *Ceram. Int.* **2021**, *47*, 20169–20177. doi:10.1016/j.ceramint.2021.04.023.

149. Lv J, Duan H, Li Y, Li Z, Yang G, Li T,Zhang S, Zhang H. Liquid-phase shear exfoliation combined with hydrothermal processing for the preparation of graphene nanosheet/AlOOH nanofiber composite powder to enhance high-temperature performance of MgO−carbon castable. *J. Eur. Ceram. Soc.* **2024**, *44*, 5896–5906. doi:10.1016/j.jeurceramsoc.2024.03.010.
150. Liu M, Huang J, Meng H, Liu C, Chen Z, Yang H, et al. A novel approach to prepare graphite nanoplatelets exfoliated by three-roll milling in phenolic resin for low-carbon MgO−C refractories. *J. Eur. Ceram. Soc.* **2023**, *43*, 4198–4208. doi:10.1016/j.jeurceramsoc.2023.02.064.
151. Li Y, Wang J, Duan H, Han L, Jia Q, Liu X. Catalytic preparation of carbon nanotube/SiC whisker bonded low carbon MgO−C refractories and their high-temperature mechanical properties. *Ceram. Int.* **2022**, *48*, 5546–5556. doi:10.1016/j.ceramint.2021.11.099.
152. Yu C, Deng C, Zhu H, Xue Z, Ding J, Zhou S. Synthesis of hexagonal plate-like $Al_4Si_2C_5$ and the effect of $Al_4Si_2C_5$ addition to Al_2O_3−C refractory. *Adv. Powder. Technol.* **2017**, 28, 177–184. doi.org/10.1016/j.apt.2016.09.012.
153. Chen J, Wei Y, Du Y, Zhang Y, Nath M, Zhang S, et al. Oxidation behaviors of low carbon MgO−C refractories: Roles of Ti_2AlC and Ti_2AlN. *J. Am. Ceram. Soc.* **2023**, *106*, 4411–4424. doi:10.1111/jace.19100.
154. Yu C, Dong B, Chen Y, Ma B, Ding J, Deng C, et al. Enhanced oxidation resistance of low-carbon MgO−C refractories with ternary carbides: A review. *J. Iron Steel Res. Int.* **2022**, *29*, 1052–1062. doi:10.1007/s42243−022−00804−5.
155. Fu Z, Pang A, Luo H, Zhou K, Yang H. Research progress of ceramic matrix composites for high temperature stealth technology based on multi-scale collaborative design. *J. Mater. Res. Technol.* **2022**, *18*, 2770–2783. doi:10.1016/j.jmrt.2022.03.164.
156. Istomin PV, Nadutkin AV, Istomina EI, Grass VE. Synthesis of Ti_3SiC_2 MAX phase ceramic materials using macrosized non-powder forms of titanium metal. *IOP Conf. Ser. Mater. Sci. Eng.* **2019**, *558*, 012015. doi:10.1088/1757−899X/558/1/012015.
157. Shen L, Eichner D, Van Der Zwaag S, Leyens C, Sloof WG. Reducing the erosive wear rate of Cr_2AlC MAX phase ceramic by oxidative healing of local impact damage. *Wear* **2016**, *358–359*, 1–6. doi:10.1016/j.wear.2016.03.019.
158. He R, Cheng X, Qu Z, Fang D. Pull-off behavior of MAX phase ceramic bolted connections: Experimental testing and simulation analysis. *Adv. Eng. Mater.* **2016**, *18*, 591–596. doi:10.1002/adem.201500288.
159. Tatarko P, Casalegno V, Hu C, Salvo M, Ferraris M, Reece MJ. Joining of CVD−SiC coated and uncoated fiber reinforced ceramic matrix composites with pre−sintered Ti_3SiC_2 MAX phase using Spark Plasma Sintering. *J. Eur. Ceram. Soc.* **2016**, *36*, 3957–3967. doi:10.1016/j.jeurceramsoc.2016.06.025.
160. Lee HM, Lee EB, Kim DL, Kim DK. Comparative study of oxide and non-oxide additives in high thermal conductive and high strength Si_3N_4 ceramics. *Ceram. Int.* **2016**, *42*, 17466–17471. doi:10.1016/j.ceramint.2016.08.051.
161. Chen W, Yu W, Ma C, Ma G, Zhang L, Wang H. A review of novel ternary nano-layered MAX phases reinforced AZ91D magnesium composite. *J. Magnes. Alloys* **2022**, *10*, 1457–1475. doi:10.1016/j.jma.2022.05.013.
162. Su J, Zhang X, Li J, Guo H, Wang B, Bai Z. Al_2O_3 fiber-reinforced MAX phase ceramic matrix composite. *Ceram. Int.* **2024**, *50*, 25400–25411. doi:10.1016/j.ceramint.2024.04.272.
163. Fu L, Xia W. MAX phases as nanolaminate materials: Chemical composition, microstructure, synthesis, properties, and applications. *Adv. Eng. Mater.* **2021**, *23*, 2001191. doi:10.1002/adem.202001191.
164. Luo J, Ding D, Xiao G. Enhanced thermal shock resistance of low-carbon Al_2O_3−C refractories by aggregate/matrix interface design with $MgAl_2O_4$/CNTs layer. *Ceram. Int.* **2024**, *50*, 13550–13561. doi:10.1016/j.ceramint.2024.01.269.
165. Li Y, Li Z, Zhai J, Zhao L, Chen J, Meng F. Synthesis, microstructure and thermal stability of graphene nanoplatelets coated by hexagonal boron nitride (h-BN). Mater. *Chem. Phys.* **2019**, *221*, 477–482. doi:10.1016/j.matchemphys.2018.09.079.
166. Liang F, Xue Z, Zhao L, Zhang H, Zhang S. Mechanical properties and thermal shock resistance of alumina/hexagonal boron nitride composite refractories. *Metall. Mater. Trans. A* **2015**, *46*, 4335–4341. doi:10.1007/s11661−015−3042−x.
167. Liu X, Chen Z, Yan W, Wang J, Ma S, Li G. A comparative study on lightweight and dense periclase-magnesium aluminate spinel refractories from industrial preparation. *J. Alloys Compd.* **2023**, *960*, 170611. doi:10.1016/j.jallcom.2023.170611.
168. Ji Z, Liu W, Liao N, Li Y, Zhu T. Influence of h-BN particle size on fracture behavior and thermal shock resistance of Al_2O_3−C refractories. *J. Iron Steel Res. Int.* **2022**, *29*, 1129–1137. doi:10.1007/s42243−022−00750−2.
169. Ji Z, Liao N, Li Y, Nath M, Zhu T, Pan L, et al. Effect of h-BN on the microstructure and fracture behavior of low carbon Al_2O_3−C refractories. *Ceram. Int.* **2021**, *47*, 29900–29907. doi:10.1016/j.ceramint.2021.07.163.
170. Zheng X, Xiao G, Li Y, Shang C, Ding D, Jin E, et al. Enhancing the thermal shock and corrosion resistance of low-carbon Al_2O_3−C refractories: The role of h-BN composite powder. *Int. J. Appl. Ceram. Technol.* **2024**, *21*, 3554–3568. doi:10.1111/ijac.14780.
171. Fan S, Deng C, Yu C, Liu Z, Ding J. Nano-laminated BN modified graphite reinforced unfired MgO−C refractories: Preparation, properties and strengthening mechanism. *J. Mater. Res. Technol.* **2024**, *29*, 4833–4844. doi:10.1016/j.jmrt.2024.02.201.
172. Li Y, Wu S, Liang F, Lv G, Tian Y, Zhang H, et al. Rod-like h-BN modified low carbon Al_2O_3−C refractory and its high-temperature service performances. *J. Eur. Ceram. Soc.* **2024**, *44*, 1825–1835. doi:10.1016/j.jeurceramsoc.2023.10.021.

173. Chen Z, Yan W, Schafföner S, Li Y, Li N. Microstructure and mechanical properties of lightweight Al_2O_3−C refractories using different carbon sources. *J. Alloys Compd.* **2021**, *862*, 158036. doi:10.1016/j.jallcom.2020.158036.
174. Li W, Zhen Q, Li R, Zhang S. Impact of in-situ SiC whisker growth on MgO−Al_2O_3−C unfired refractories. *Ceram. Int.* **2024**, *50*, 7682–7690. doi:10.1016/j.ceramint.2023.12.092.
175. Chen Y, Ding J, Deng C, Yu C. Improved thermal shock stability and oxidation resistance of low-carbon MgO−C refractories with introduction of SiC whiskers. *Ceram. Int.* **2023**, *49*, 26871–26878. doi:10.1016/j.ceramint.2023.05.224.
176. Li Y, Bi Y, Liu X, Dong L, Cai W, Lv J, et al. Preparation and properties of alumina-carbon castables using SiC nanofiber coated graphite flake. *Appl. Surf. Sci.* **2023**, *615*, 156275. doi:10.1016/j.apsusc.2022.156275.
177. Liu Z, Deng C, Yu C, Wang X, Ding J, Zhu H. Preparation of in-situ grown silicon carbide whiskers onto graphite for application in Al_2O_3−C refractories. *Ceram. Int.* **2018**, *44*, 13944–13950. doi:10.1016/j.ceramint.2018.04.243.
178. Ban J, Zhou C, Feng L, Jia Q, Liu X, Hu J. Preparation and application of ZrB_2−SiCw composite powder for corrosion resistance improvement in Al_2O_3−ZrO_2−C slide plate materials. *Ceram. Int.* **2020**, *46*, 9817–9825. doi:10.1016/j.ceramint.2019.12.255.
179. Liu G, Liao N, Nath M, Li Y, Sang S. Optimized mechanical properties and oxidation resistance of low carbon Al_2O_3−C refractories through Ti_3AlC_2 addition. *J. Eur. Ceram. Soc.* **2021**, *41*, 2948–2957. doi:10.1016/j.jeurceramsoc.2020.11.038.
180. Chen J, Wu Z, Li B, Deng M, Yan W, Wei Y, et al. Influence of Cr_2AlC on the thermal shock and corrosion resistance of low carbon Al_2O_3−C refractory. *J. Eur. Ceram. Soc.* **2024**, *44*, 7943–7952. doi:10.1016/j.jeurceramsoc.2024.05.048.
181. Luo Y, Liu Z, Yu C, Deng C, Ding J. Enhanced service performances of in-situ Mg−Sialon/$MgAl_2O_4$ folding structure in low carbon Al_2O_3−C refractories: Phase reconfiguration of nano-$MgSiN_2$. *J. Eur. Ceram. Soc.* **2024**, *44*, 7953–7968. doi:10.1016/j.jeurceramsoc.2024.05.066.
182. Lu Z. Theoretical screening, intrinsic brittleness and thermal properties of the S-containing MAX carbides and borides. *J. Mater.* **2023**, *9*, 1056–1066. doi:10.1016/j.jmat.2023.04.005.
183. Wu S, Xu X, Yang S, Qiu J, Volinsky AA, Pang X. Data−driven optimization of hardness and toughness of high-entropy nitride coatings. *Ceram. Int.* **2023**, *49*, 21561–21569. doi:10.1016/j.ceramint.2023.03.292.
184. Qi X, Luo X, Zhang L, Wang S, Zhao J. In situ synthesis and interfacial bonding mechanism of SiC in MgO−SiC−C refractories. *Int. J. Appl. Ceram. Technol.* **2022**, *19*, 2723–2733. doi:10.1111/ijac.14072.
185. Li X, Badie S, Gonzalez−Julian J, Schwaiger R, Malzbender J. Abrasive behavior of M_2Al_X MAX phase materials and its relation to the brittleness index. *Ceram. Int.* **2022**, *48*, 19501–19506. doi:10.1016/j.ceramint.2022.03.196.
186. Liang H, Lin W, Wang Q, Zhang W, Guan S, Zhang J, et al. Ultrahard and stable nanostructured cubic boron nitride from hexagonal boron nitride. *Ceram. Int.* **2020**, *46*, 12788–12794. doi:10.1016/j.ceramint.2020.02.048.
187. Li X, Cao T, Zhang M, Qiu H, Huang Y, Qu S, et al. Ultrafine porous boron nitride nanofiber-toughened WC composites. *Int. J. Appl. Ceram. Technol.* **2020**, *17*, 941–948. doi:10.1111/ijac.13466.
188. Chen X, Bei G. Toughening mechanisms in nanolayered MAX phase ceramics−A review. *Materials* **2017**, *10*, 366. doi:10.3390/ma10040366.
189. Fan L, Cai X, Wang H, Wang F, Song F. Carbon nanotubes at the graphene/h-BN interface abnormally enhance its fracture toughness. *Diam. Relat. Mater.* **2024**, *141*, 110662. doi:10.1016/j.diamond.2023.110662.
190. Sawunyama L, Oyewo OA, Seheri N, Onjefu SA, Onwudiwe DC. Metal oxide functionalized ceramic membranes for the removal of pharmaceuticals in wastewater. *Surf. Interfaces* **2023**, *38*, 102787. doi:10.1016/j.surfin.2023.102787.
191. Zhang P, Lou Z, Gong L, Wu Z, Chen X, Xu W, et al. Development and applications of thermoelectric oxide ceramics and devices. *Energies* **2023**, *16*, 4475. doi:10.3390/en16114475.
192. Chen S, Chen Y, Zhao Y, Zhang L, Zhu C, Zhang Y, et al. Status and strategies for fabricating flexible oxide ceramic micro-nanofiber materials. *Mater. Today* **2022**, *61*, 139–168. doi:10.1016/j.mattod.2022.11.004.
193. Aparicio IE, Fishpool DT, Diaz VR, Dorey RA, Yeomans JA. Evaluation of polymer matrix composite manufacturing routes for production of an oxide/oxide ceramic matrix composite. *J. Eur. Ceram. Soc.* **2022**, *42*, 2420–2428. doi:10.1016/j.jeurceramsoc.2021.12.059.
194. Hannachi E, Sayyed MI, Almuqrin AH, Mahmoud KG. Study of the structure and radiation-protective properties of yttrium barium copper oxide ceramic doped with different oxides. *J. Alloys Compd.* **2021**, *885*, 161142. doi:10.1016/j.jallcom.2021.161142.
195. Ye B, Kim E−S, Cui M, Khim J, Baik JM, Kim H−D. Fine-structured oxide ceramics from a novel replication method. *Ceram. Int.* **2016**, *42*, 10872–10878. doi:10.1016/j.ceramint.2016.03.218.
196. Duan J, Han B, Wei J, Chen C, Miao Z, Wang H, et al. Corrosion mechanism and microstructure evolution of industrial used Al_2O_3−ZrO_2−C slide plates. *Mater. Today Commun.* **2024**, *39*, 108796. doi:10.1016/j.mtcomm.2024.108796.
197. Jia X, Tian L, Mao S, Zhou X, Chen S, Li G. Slag erosion-resistant coating for periclase−magnesia−aluminum spinel brick. *Ceram. Int.* **2021**, *47*, 31407–31412. doi:10.1016/j.ceramint.2021.08.016.
198. Kusiorowski R. MgO−ZrO_2 refractory ceramics based on recycled magnesia−carbon bricks. *Constr. Build. Mater.* **2020**, *231*, 117084. doi:10.1016/j.conbuildmat.2019.117084.

199. Navarro RCS, De Avillez RR, Goes TF, Gomes AMS. Low temperature thermal and volumetric behavior of $MnAl_2O_4$ spinel. *J. Mater. Res. Technol.* **2020**, *9*, 4194–4205. doi:10.1016/j.jmrt.2020.02.046.
200. Li Y, Meng X, Chen K, Barati M. Crystallization behaviors of spinel during cooling process of modified EAF slag. *Metall. Mater. Trans. B* **2020**, *51*, 1027–1038. doi:10.1007/s11663−020−01802−2.
201. Sarkar R, Sohn HY. Interactions of alumina-based and magnesia-based refractories with iron melts and slags: A review. *Metall. Mater. Trans. B* **2018**, *49*, 1860–1882. doi:10.1007/s11663−018−1300−1.
202. Roungos V, Aneziris CG. Improved thermal shock performance of Al_2O_3−C refractories due to nanoscaled additives. *Ceram. Int.* **2011**, *38*, 919–927. doi:10.1016/j.ceramint.2011.08.011.
203. Ghasemi−Kahrizsangi S, Dehsheikh HG, Boroujerdnia M. Effect of micro and nano-Al_2O_3 addition on the microstructure and properties of MgO−C refractory ceramic composite. *Mater. Chem. Phys.* **2017**, *189*, 230–236. doi:10.1016/j.matchemphys.2016.12.068.
204. Zhu T, Li Y, Sang S, Jin S, Wang H. Formation of hollow MgO-rich spinel whiskers in low carbon MgO−C refractories with Al additives. *J. Eur. Ceram. Soc.* **2014**, *34*, 4425–4432. doi:10.1016/j.jeurceramsoc.2014.07.028.
205. Das RR, Nayak BB, Adak S, Chattopadhyay AK. Influence of nanocrystalline $MgAl_2O_4$ spinel addition on the properties of MgO−C refractories. *Mater. Manuf. Process.* **2012**, *27*, 242–246. doi:10.1080/10426914.2010.544958.
206. Gu Q, Zhao F, Liu X, Jia Q. Preparation and thermal shock behavior of nanoscale $MgAl_2O_4$ spinel-toughened MgO-based refractory aggregates. *Ceram. Int.* **2019**, *45*, 12093–12100. doi:10.1016/j.ceramint.2019.03.107.
207. Gu Q, Ma T, Zhao F, Jia Q, Liu X, Liu G, et al. Enhancement of the thermal shock resistance of MgO−C slide plate materials with the addition of nano-ZrO_2 modified magnesia aggregates. *J. Alloys Compd.* **2020**, *847*, 156339. doi:10.1016/j.jallcom.2020.156339.
208. Dehsheikh HG, Ghasemi−Kahrizsangi S. Performance improvement of MgO−C refractory bricks by the addition of Nano-$ZrSiO_4$. *Mater. Chem. Phys.* **2017**, *202*, 369–376. doi:10.1016/j.matchemphys.2017.09.055.
209. Ghasemi−Kahrizsangi S, Dehsheikh HG, Karamian E. Impact of Titania nanoparticles addition on the microstructure and properties of MgO−C refractories. *Ceram. Int.* **2017**, *43*, 15472–15477. doi:10.1016/j.ceramint.2017.08.094.
210. Chen Q, Zhu T, Li Y, Cheng Y, Liao N, Pan L, et al. Enhanced performance of low-carbon MgO−C refractories with nano-sized ZrO_2−Al_2O_3 composite powder. *Ceram. Int.* **2021**, *47*, 20178–20186. doi:10.1016/j.ceramint.2021.04.024.